Thermal Model of an Annular Fuel Cell

by

Guillermo Urquiza Fernandez

SUBMITTED TO THE DEPARTMENT OF MECHANICAL ENGINEERING
IN PARTIAL FULFILLMENT OF THE REQUIREMENTS FOR THE DEGREES OF

BACHELOR OF SCIENCE

AND

MASTER OF SCIENCE IN MECHANICAL ENGINEERING

AT THE
MASSACHUSETTS INSTITUTE OF TECHNOLOGY
FEBRUARY 2003

Signature of Author.....
.....
Department of Mechanical Engineering
December 16, 2002

Certified by.....
.....
Joseph L. Smith
Collins Professor of Mechanical Engineering
Thesis Supervisor

Accepted by.....
.....
Ain A. Sonin
Chairman, Department Committee on Graduate Students

Thermal Model of an Annular Fuel Cell

by

Guillermo Urquiza Fernandez

Submitted to the Department of Mechanical Engineering
on December 16, 2002 in Partial Fulfillment of the
Requirements for the Degrees of Bachelor of Science and
Master of Science in Mechanical Engineering

Abstract

A fuel cell is an electrochemical device that converts diatomic hydrogen and diatomic oxygen into water, electricity, and heat via an electrolyte. Different electrolytes function within different temperature ranges and are very sensitive to shifts outside the range. As such, the temperature inside a fuel cell must be very carefully controlled. The fuel cell in question has an annular geometry and has hot fluid running through the bore. This report composes three thermal models of the system that show the proposed geometry is satisfactory with respect to the heat transfer inside the fuel cell.

Thesis Supervisor: Joseph L. Smith
Title: Collins Professor of Mechanical Engineering

Acknowledgements

First of all, I would like to thank my family for their loving support throughout the course of my studies. I would also like to thank my friends for the help they gave me in my times of need. You guys the badest.

In particular, I thank Alfonso Romo for the support he and Pulsar Intl. bestowed upon me for my undergraduate studies. I will never forget that; and I greatly appreciate it. With luck, someday I may be able to help someone in their education.

In addition I would like to thank Schlumberger for the fantastic Internship experience. In particular Wenlin Zhang, Joe Walter, Albert Perez, and Christian Garcia for the aid and support they provided in producing this thesis. And special thanks must go to Carclos Sanchez and Lavish Mongue for the enlightening living experience.

Lastly I would like to thank Prof. Joseph Smith for the advice and guidance he provided throughout my undergraduate and graduate education.

Table of Contents

List of Figures

1. Introduction

A fuel cell is an electrochemical device that harnesses the energy associated with oxidizing hydrogen atoms to form water molecules and converting it into electrical energy. It does this setting up a chemical and electrical potential across an electrolyte layer and passing electrons through a circuit across the membrane.

The following section is a short discussion as to the background necessary to deal with any fuel cell apparatus. It specifies how a fuel cell works, with emphasis on a PEM fuel cell; the purpose for this particular application; and the purpose for a thermodynamic model of an annular fuel cell.

1.1 How a fuel cell works. The PEM fuel cell

At the heart of any fuel cell is the design of its electrolyte and catalyst system. In a Polymer Electrolyte Membrane (PEM) fuel cell, this system consists of five layers: an anode, a catalyst layer, a polymer membrane, another catalyst layer, and a cathode. This makes up the Membrane-Electrode-Assembly (MEA).

Diatomic hydrogen enters the fuel cell on the anode side of the membrane and is separated into its monatomic form by a porous platinum catalyst layer. The electrons stripped from the protons then pass through an external circuit; at the same time, hydrogen ions are allowed through the polymer membrane. On the cathode side, diatomic oxygen has been split into its monatomic form by the catalyst. The oxygen, electrons, and hydrogen protons unite to form heat and water which is then removed from the fuel cell as the cycle continues.

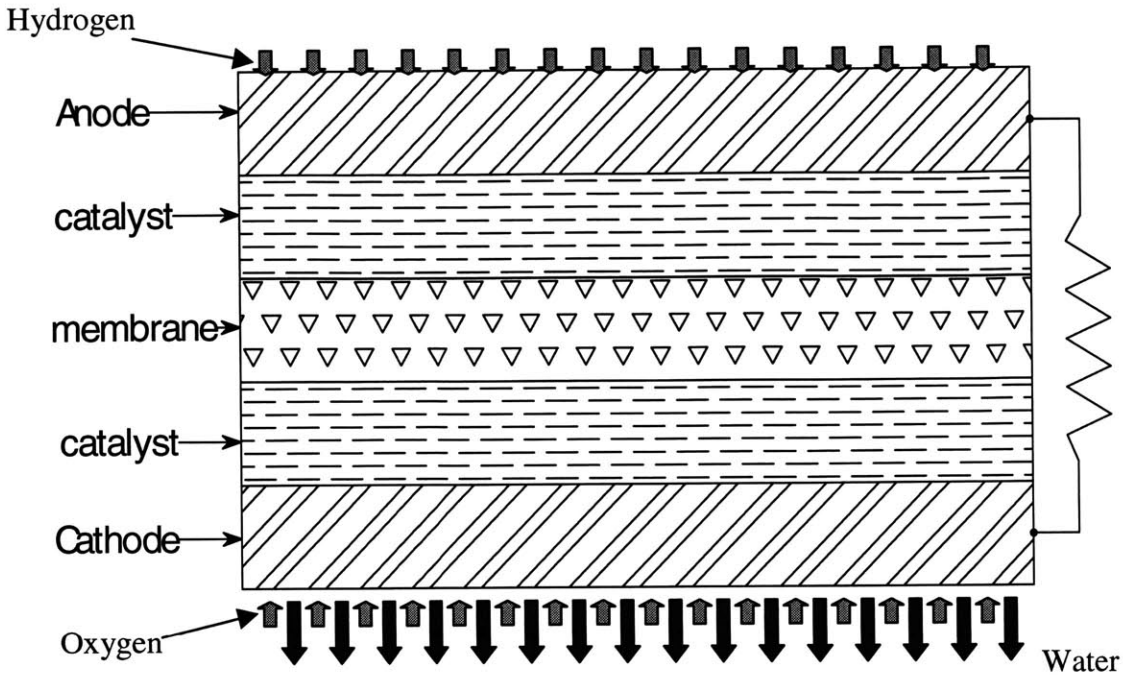

Figure 1: The PEM Fuel Cell

A PEM fuel cell is different from other fuel cells in that it has a polymer membrane designed to transport hydrogen protons across itself while the electrons traverse an external circuit. Different types of fuel cells utilize different electrolyte properties to operate in different temperature ranges, for different current densities, and different operating situations.

In all, the reaction consists of diatomic hydrogen and diatomic oxygen as its reactants, and water, electricity, and heat as its products:

$$H_2 + \frac{1}{2}O_2 \rightarrow H_2O + P_{elec.} + \dot{Q}_{gen}$$

The area of the Membrane-Electrode-Assembly (referred to from here on as the MEA) that is actually in contact with this reaction is also known as the active area. The larger the area, the

larger the power output proportionally. For this reason, many times cells are stacked in series. Stacking cells serially provides larger active areas and therefore higher voltages (and therefore larger power output) while maintaining geometric feasibility.

When stacking cells, the anode and the cathode of the stack are at either extreme. However, each cell must have its own anode and cathode in order for the necessary potential for the reaction to exist. This is accomplished via the notion of a bipolar plate. To illustrate this, take for example, the simplest form of a stack: a two-celled stack.

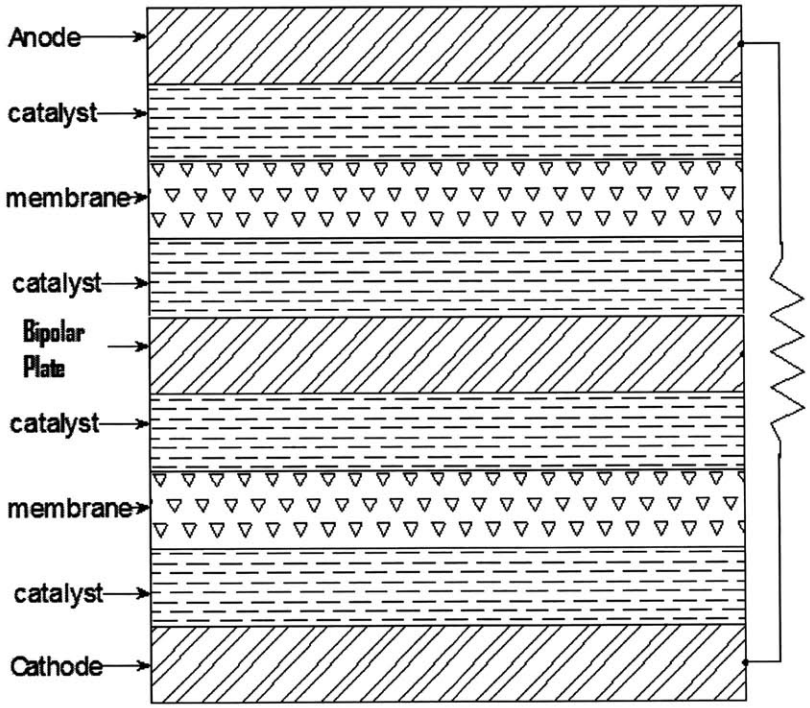

Figure 2: Two-cell stack

Figure 2 depicts a stack consisting of an anode, an MEA, a bipolar plate, another MEA, and a cathode. The function of the bipolar plate is to maintain the potential between the first cell and the second cell without shorting the two cells. It separates the two reactions performing in parallel, but connected serially. On the upper surface of the bipolar plate, the 2nd half of the

reaction takes place with water being drained from the 1st cell. On the lower surface, the first half of the reaction takes place with the channeling of hydrogen into the 2nd cell. Intuitively, if the potential of one cell is X, the potential created by a two cell stack is 2X. Therefore, the potential of a cell stack is directly proportional to the number of cells in the stack.

1.2 The application

In the Oil-field industry, it is necessary to provide a source of electrical power to instruments and tools inside a well. The current source of power is located, in many cases on a ship in the middle of the ocean. Power is conveyed down-hole by what is known in the Oil-field industry as an umbilical. This is a massive extension that travels from a power source on a ship or rig all the way down to the bottom of the sea. In some cases this can be up to 10,000 feet. Not mentioning the variation in depth from one site to the next, one of these umbilicals is extremely cumbersome and expensive. Weather also plays a role in the difficulty of these umbilicals. Rough seas can force a rig or ship to cut off its umbilical in order to save the integrity of the well below. Needless to say, eliminating the umbilical all together would benefit production tremendously.

In order to eliminate the umbilical, one must provide power to all the down-hole equipment that previously depended on the umbilical. A fuel cell's power density, versatility, and ability to function with constant supplies of fuel are ideal for this application.

1.3 The proposed setup

The purpose of the fuel cell is to power sub-sea equipment from the ocean floor for oil-drilling applications. To shield the fuel cell and other equipment from the harsh environments of

the ocean floor a long tube, known as a riser, extends from the sea surface to the sea floor. This is filled with liquid known as drilling mud and brine to help isolate the produced fluid from the environment. Another long tube or manifold runs along the axis of the riser to the rig or ship. The produced fluid runs directly through the manifold from the well to the ship. Therefore, the only space the fuel cell would fit is the annular gap between the manifold and the riser. Figure 3 illustrates the arrangement of the fuel cell with respect to its surroundings.

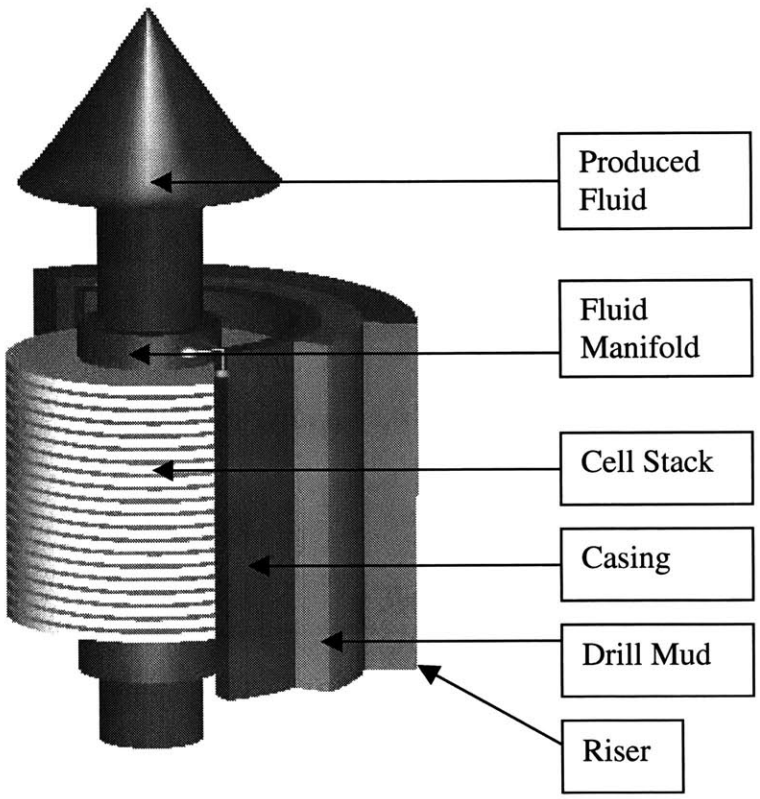

Figure 3: Cut-out of Fuel cell with its surroundings

The setup of the riser is fixed due to the cost and effort necessary to redesign the entire assembly. Therefore, the fuel-cell dimensions are constrained to the region between the inner diameter of the riser and the outer diameter of the manifold. To maximize the active area, an annular fuel cell must be used.

The basic design that has been proposed, and for which this report will conduct analysis is depicted in Figure 4 and defined in the next section.

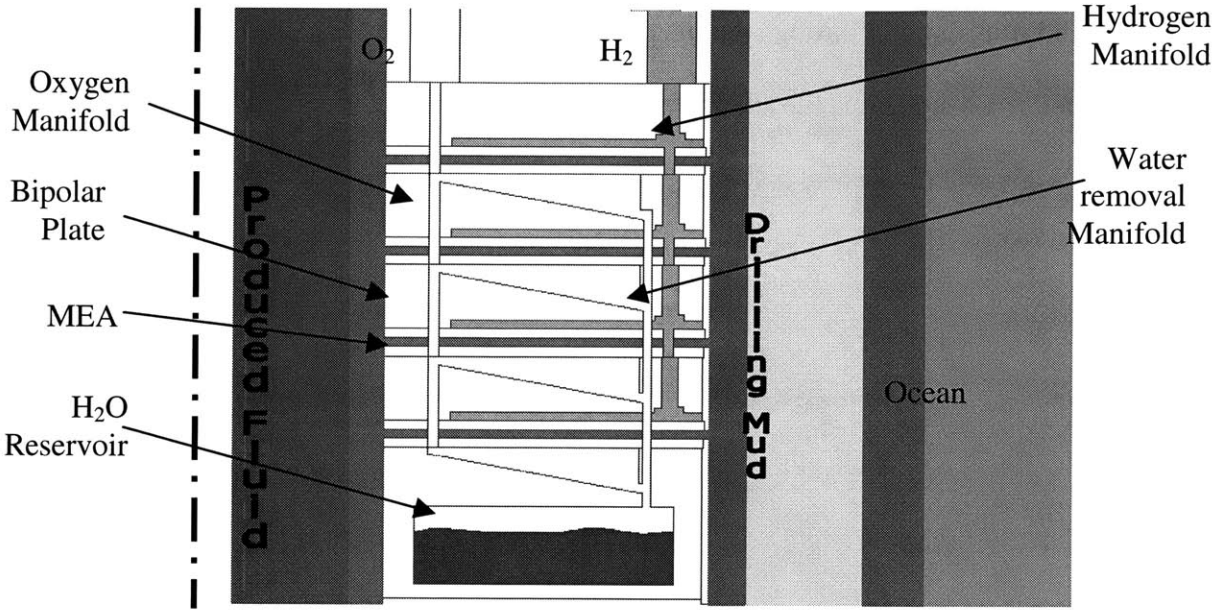

Figure 4: Half cross-section of the annular fuel cell and its surroundings

1.4 The DUCS fuel cell.

The Deep-sea Umbilicalless Control System (referred to from here on as the DUCS fuel cell) is composed of a number of confidential components that are not relevant to this study and will not be detailed in this report. The DUCS fuel cell is the focus. It is composed of 50 MEA's (Membrane Electrolyte Assemblies) providing each a calculated 10 Watts for a total of 500 Watts.

Figure 4 illustrates a simplified half cross-section of the setup. To the left of the dashed center-line would be a mirror image of the picture to the right of it. The left side of the cross-section was left out for simplicity.

The main bulk of the fuel cell is comprised of the 51 graphite plates stacked on top of each other (49 bipolar plates and two end-plates). These plates are made of specially coated and baked graphite to prevent the graphite's porous structure from leaking volatile hydrogen into the surrounding environment. The reason graphite was chosen as the material for the bipolar plates is for its light weight, high electrical conductivity, and high thermal conductivity.

Each bipolar plate has 16 oxygen manifolds and 24 hydrogen manifolds and 8 water removal manifolds drilled into it axially on its inner and outer rings. These numbers are strictly for even distribution of the gasses throughout the cavities of the fuel cell and do not affect the flow rates since the flow across the membrane is relatively low compared to the capacity of the manifolds.

Figure 5: Top (oxygen side) of the bipolar plate

Figure 5 depicts the top surface of a bipolar plate. The "top" of the plate is actually the side that sees the oxygen and water. The "bottom" of the plate is very similar with the exception that the slots do not have a downward slope. They are one sixteenth of an inch deep and flat.

Each bipolar plate also has 120 two degree wide interconnected slots milled into its lower surface to allow the hydrogen to distribute itself on the upper side of the MEA. The space between slots is one degree wide and is used to provide support for the MEA and to conduct electricity from the electrode. Each plate also has 120 downward-sloped slots milled into its upper surface (see figure 4). The purpose for the slope is so that gravity can pull water that is

generated by the reaction out of the each cell through the water removal manifolds into a reservoir.

There are 49 of the bipolar plates. The other 2 plates are end plates which are basically the same as a bipolar plate on one side but the top plate only has the hydrogen side and the bottom plate only has the oxygen side milled. The outer surfaces act as an interface to the rest of the DUCS system. For the purposes of this analysis, only the bipolar plates will be modeled.

2. Thermal Issues

2.1 The Nafion® membrane

The membrane is made of Polytetrafluoroethylene (Nafion® is Dupont's trademarked name). It is basically a polymer doped with ions that, when hydrated, permits other ions to pass by passing them along a chain of hydrogen bonds.

Figure 6: Picture of internal structure

The structure of the Nafion(R) membrane is, for the most part, amorphous. However, in the presence of positive ions, the water molecules form "columns" that permit hydrogen to pass through its structure, thereby allowing a certain conduction created by the reaction potential.

Since water is a very critical component of the ion transport, this membrane is very susceptible to dehydration. In ambient pressure, the PEM membrane's ion conductivity drops significantly as temperature goes to about 100 deg C. The DUCS Fuel Cell is designed to have the hydrogen and oxygen at a static pressure of 60 PSI; this increases the vaporization temperature of water. Therefore, dehydration of the membrane does not begin to take a toll on

the efficiency of the fuel cell until temperatures of about 120 deg C are reached. More information about the Nafion® membranes can be found in Appendix B

2.2 Heat Transfer into cells

It is now established that the PEM fuel cell is very susceptible to temperature changes. This particular design geometry lends itself to significant influence from outside heat transfer. Since the well-bore runs through the fuel cell itself, and down-hole temperatures can be volatile, temperature control is still a crucial facet of this fuel cell project. An increase of ten degrees Celsius could dramatically affect the efficiency of the fuel cell. There are three major ways that heat is transferred to a cell: 1) Heat transfer from produced fluid; 2) Heat transferred from the reaction inside the cell; 3) Heat dissipated from the cell, to the housing, and into the drilling mud. These three modes of heat transfer are depicted in Figure 7.

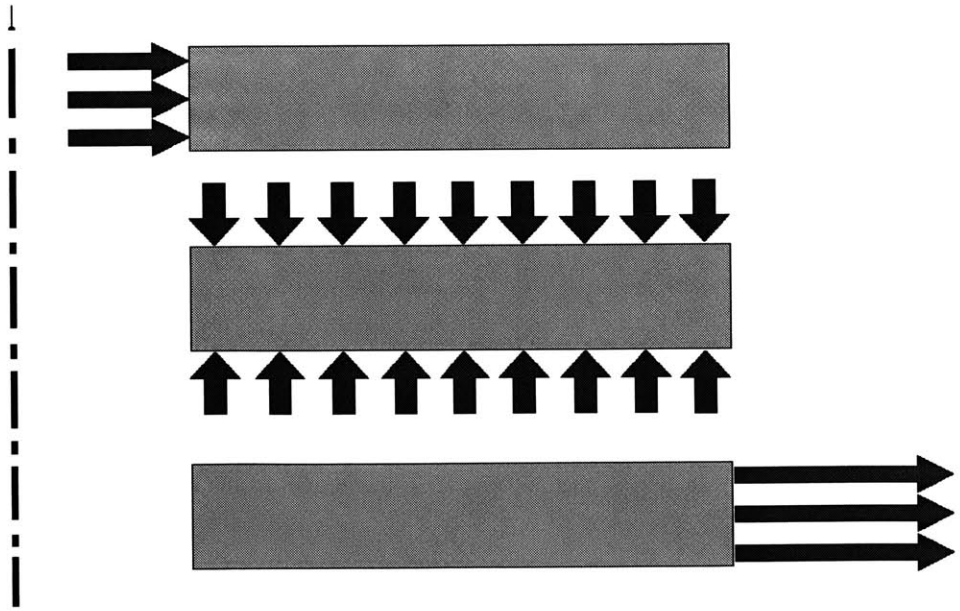

Figure 7: 3 Modes of Heat Transfer into a Cell

3. 1-D Thermal Model

3.1 Governing equations and assumptions

$$\frac{1}{r}\frac{\partial}{\partial r}(kr\frac{\partial T}{\partial r})+\frac{1}{r^2}\frac{\partial}{\partial \phi}(k\frac{\partial T}{\partial \phi})+\frac{\partial}{\partial z}(k\frac{\partial T}{\partial z})+\dot{q}=\rho c_p\frac{\partial T}{\partial t} \tag{1}$$

Equation 1 is the conduction heat equation for solid (no fluid flow) radial systems. The first term is the heat conducted radially from the center. The next term denotes heat transfer in the tangential direction. The third term is the heat transferred axially. Finally, the last term on the left side of the equation represents the heat generated per unit volume of the cylinder. Lastly, the term on the left side of the equation indicates the effect of time. For the 1-D Model, the following assumptions were made for simplicity:

1. The geometry of the bipolar plates was assumed to be a solid disk. The conduction resistance created because of the slots in the plate, were assumed to be negligible.
2. Constant material properties (such as thermal conductivity) are present throughout any given cross section in the plate.
3. A cylindrical coordinate system was used (see figure 8), and heat transfer in the phi direction was neglected because of symmetry. Again, there would be a difference between the heat transfer along a slot, and the heat transfer along a channel wall; but this was deemed negligible for these purposes and will be analyzed more deeply in the 2-D model.
4. Heat transfer in the z direction was also considered negligible. This is because each bipolar plate has a reaction occurring on both of its sides. Hence, the heat transferred into the bipolar plate is conducted to the exterior edge of the plate.
5. Steady state conditions were assumed.

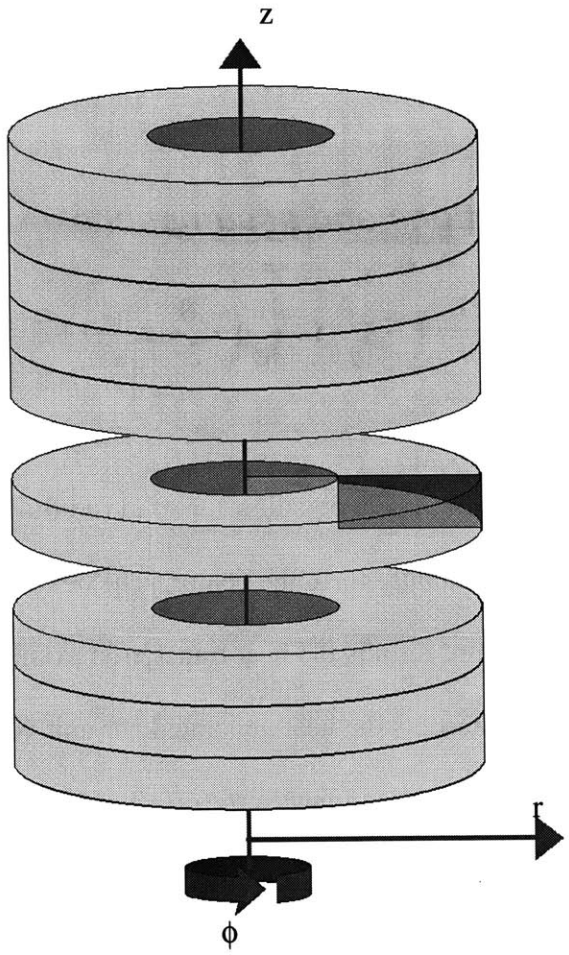

Figure 8: Coordinate system and cross section of bipolar plate considered.

Under these assumptions, the heat conduction equation can be simplified to

$$\frac{k}{r}\frac{\partial}{\partial r}\left(r\frac{\partial T}{\partial r}\right)+\dot{q}=0 \tag{2}$$

From here, the heat equation was solved for the temperature distribution. The heat generated by the reaction was used in this model to see how the distribution affects the temperature of the bipolar plate per unit volume. For this case, the Heat Generated, Q, is divided by the volume of the solid annular disk of inside radius R_1. This assumes that the total heat generated is uniformly

distributed throughout the volume defined by R_1, R_2, and h. Where R_1 and R_2 are the inner and outer radii respectively

$$\frac{k}{r}\frac{\partial}{\partial r}\left(r\frac{\partial T}{\partial r}\right)+\frac{\dot{Q}_{gen}}{\pi(R_2^{\,2}-R_1^2)h}=0 \tag{3}$$

The following steps are comprised of the integration and the manipulation involved in solving for the temperature distribution. For this reason, they will not be numbered.

$$\frac{\partial}{\partial r}\left(r\frac{\partial T}{\partial r}\right)+\frac{\dot{Q}_{gen}r}{\pi kh(R_2^{\,2}-R_1^2)}=0$$

$$r\frac{\partial T}{\partial r}+\frac{\dot{Q}_{gen}r^2}{2\pi kh(R_2^{\,2}-R_1^2)}+C_1=0$$

$$\frac{\partial T}{\partial r}+\frac{\dot{Q}_{gen}r}{2\pi kh(R_2^{\,2}-R_1^2)}+\frac{C_1}{r}=0$$

$$T(r)+\frac{\dot{Q}_{gen}r^2}{4\pi kh(R_2^{\,2}-R_1^2)}+C_1\ln(r)+C_2=0$$

Solving for the constants of integration using the boundary conditions of T(R1)=T1 and T(R2)=T2, one can arrive at a temperature distribution for the annular disk:

$$T(r)=-\frac{\dot{Q}_{gen}r^2}{4\pi kh(R_2^{\,2}-R_1^2)}-\frac{\ln(r)}{\ln(R_1/R_2)}\left[T_2-T_1+\frac{\dot{Q}_{gen}}{4\pi kh}\right]+$$
$$\frac{\dot{Q}_{gen}R_1^2}{4\pi kh(R_2^{\,2}-R_1^2)}+\frac{\ln(R_1)}{\ln(R_1/R_2)}\left[T_2-T_1+\frac{\dot{Q}_{gen}}{4\pi kh}\right]+T_1=0 \tag{4}$$

Where, R1 is the inner radius, R2 is the outer radius, Q is the total heat generated in the volume by the reaction, T1 is the temperature on the inner radius, T2 is the temperature on the outer radius, k is the thermal conductivity of the material, and h is the height of the annular disk.

3.2 1-D Steady-State Results

Figure 9 represents the temperature distribution calculated in an annular disk with internal temperature of 400K and external temperature of 300K generating 10W of internal heating. The geometry and material properties used are on the table in figure 8.

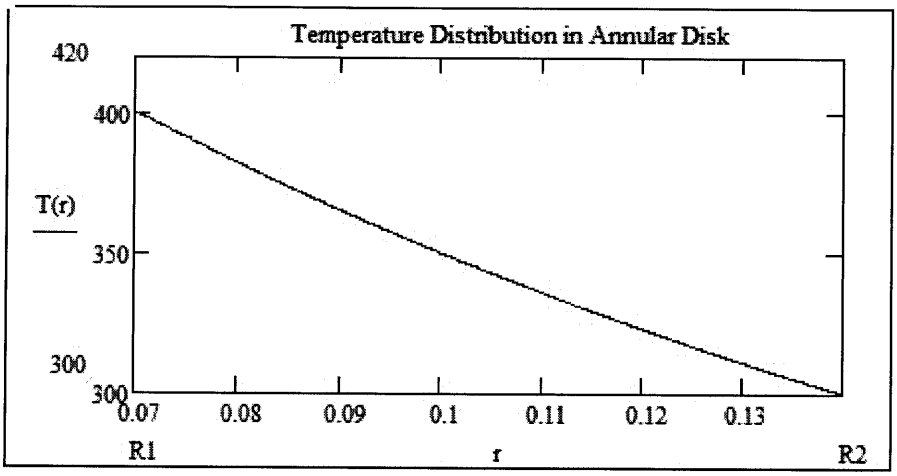

Qdot [W]	10
k [W/(mK)]	167.36
R1 [m]	0.06985
R2 [m]	0.1397
T1 [K]	400
T2 [K]	300
h [m]	0.0127

Figure 9: 1-D Steady State Results.

The boundary conditions chosen for these results include adiabatic upper and lower surfaces; ID temperature of 400 K; and OD temperature of 300 K. The upper and lower surfaces are deemed adiabatic because there is a constant heat flux of about 10 W from the heat generated by the reaction. This heat is distributed uniformly about the upper and lower surfaces; and the disk is one of many identical disks stacked vertically; therefore, there is no heat flux in the z-direction. Thus, these surfaces are adiabatic. The ID and OD temperatures were chosen based on estimates made by field experts.

4. 2-D model

The one-dimensional model gave satisfactory results in terms of the heat transfer through the bipolar plates assuming the assumptions that were made were correct. The next phase in the analysis will test the validity of the third assumptions. Namely that the heat transfer difference between the wall and the groove is negligible. To determine the effects of the groove, take into consideration a worst-case scenario where the entire disk that is conducting the heat is actually a cone as in figure 10a.

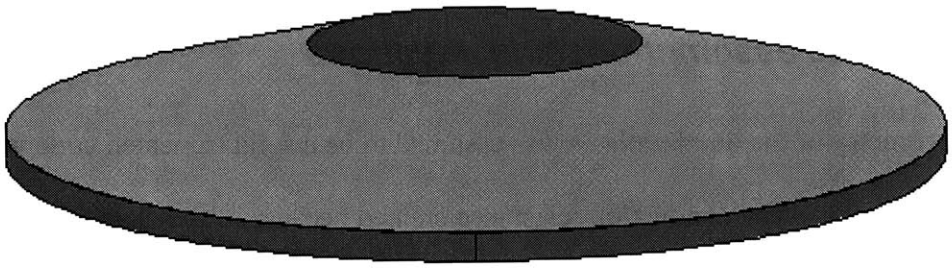

Figure 10a: Truncated and Bored cone

This geometry has a decreasing dimension in the z-direction while having the increasing dimension radially as in figure 10b. The 1-D model's geometry did not take into account the decreasing z-dimension. Therefore, the hypothesis to be tested here is that the effects of the decreasing z-dimension are in fact, negligible.

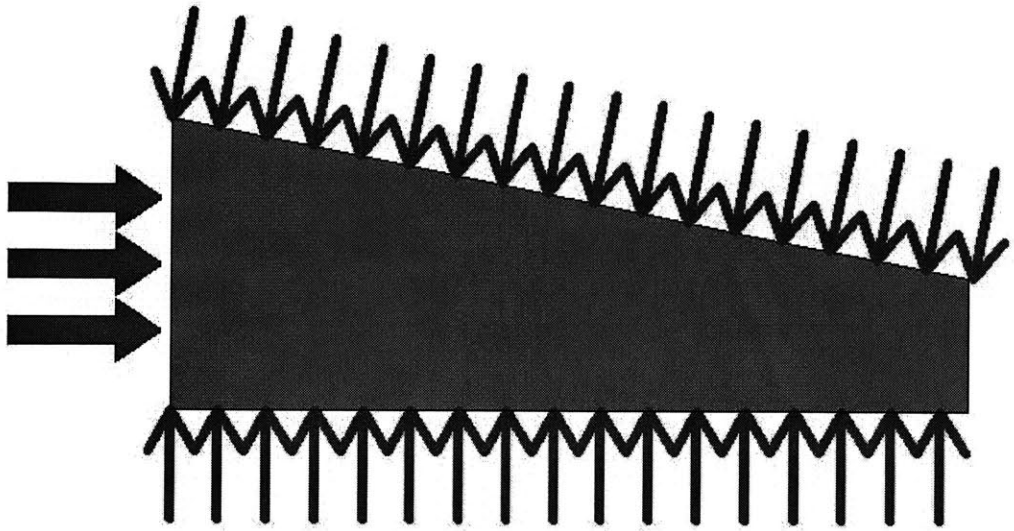

Figure 10b: X-section of the truncated cone

4.1 Governing assumptions and equations

1. The geometry of the bipolar plates was assumed to be a solid truncated cone with a whole through its axis. The conduction resistance created because of the slots in the plate, were assumed to be smoothed out and adequately represented by the z-taper of the cone.
2. Constant material properties (such as thermal conductivity) are present throughout any given cross section in the plate.
3. A cylindrical coordinate system was used (see figure 8), and heat transfer in the phi direction was neglected because of symmetry.
4. Heat transfer in the z direction was considered in this model. The decreasing height of the cone as position radially increases is taken into account.
5. Steady state conditions were assumed.

Like in the one-dimensional model, the governing heat transfer equation for the 2-dimensional case will be equation 1. However, take into consideration the definition of heat flux for radial conduction:

$$q = kA\frac{\partial T}{\partial r} \tag{5}$$

Where k is the thermal conductivity, T is the temperature, q is the heat flux, and A is the cross-sectional area as a function of r: $2\pi r(a+br)$ where b is the slope of the grove and a is the intersection of the slope with the axis. We know that $\frac{\partial q}{\partial r} = 0$ from continuity and the assumption of uniform thermal properties. Taking the partial derivative with respect to r, we get

$$\frac{\partial q}{\partial r} = \frac{\partial}{\partial r}\left[2\pi kr(a+br)\frac{\partial T}{\partial r}\right] = 0$$

$$2\pi k\left[r(a+br)\frac{\partial^2 T}{\partial r^2} + \frac{\partial T}{\partial r}(a+2br)\right] = 0$$

$$\frac{\partial^2 T}{\partial r^2} + \frac{\partial T}{\partial r}\frac{(a+2br)}{r(a+br)} = 0 \tag{6}$$

This is a simple second order differential equation which can be solved and plotted to find the temperature distribution as a function of r for a truncated cone as in figure 10a and 10b.

4.2 Results

Figure 11 shows the results of the quasi-2-dimensional model. Equation 6 was solved and plotted by mathcad to output the graph. The solid line depicts the results of the annular disk

from the 1-D model. Superimposed on this graph is the result of the 2-D model in a dashed line. One can clearly see that there is no clear distinction between the two lines; they are directly on top of each other. Indeed, the two differ by only tenths of a degree for any given position in r. This proves that the effects of the water removal slope with respect to thermal conductivity for a given cross-section are negligible.

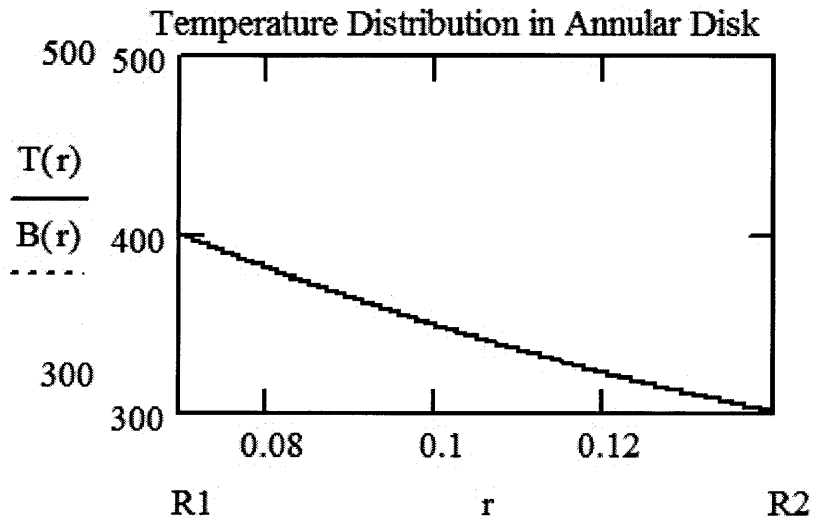

Figure 11: T(r)= temp. dist. in 2-D model; B(r)=temp. dist. in 1-D model

5. 3-dimensional FEA model

5.1 Finite Element Analysis methods

There are many different approaches to a finite element problem. The basic idea is to divide the body that is to be analyzed into more workable elements. In this way, one can analyze the basic governing equations of the process being analyzed on each element and using the principles of continuity and conservation, relate each element to its neighboring elements.

Proengineer Mechanica was the FEA packaged chosen for the analysis of the bipolar plate for its simplicity and its availability at Schlumberger. One thing to note about this package, is that unlike many other packages (Ansys, Abacus, etc.) Mechanica is what is known as a P-type FEA package. Ansys, Abacus and most others are H-type. The difference comes in the approach of the analysis. When considering the body as a whole, an FEA package divides the body into many small elements, as mentioned above. To attain greater semblance to the natural process, an H-type process divides the already existing elements into smaller elements using the same equations as on the previous model. This basically refines the output into many, more discrete, segments.

A P-type process (such as Mechanica) on the other hand, increases the polynomial order of the equations being analyzed to achieve greater semblance. This leads to the possibility of error-generation if the software chooses an element order that is not compatible with the mesh density. The following sections go through the creation of the mesh; which is imperative to the accuracy of the FEA. Following this is the details about the boundary conditions specified; and, finally, the results of the analysis.

5.2 Descretizing the bipolar plate

To simplify this analysis, it is possible to divide the bipolar plate into pieces that have the same temperature distribution. The bipolar plate is a disk with a hole along its axis. It has a series of identical grooves machined into it angularly about its axis. From symmetry, it is clear to see that at any point inside one groove, the temperature at the same position within another groove will be the same.

The dimensions of each groove are angular. Each groove is two degrees wide and each wall is 1 degree thick. Therefore there are 120 grooves in each bipolar plate. This means that for any position in z, as θ goes from 0 to 2π, the temperature will go through 120 cycles. Thus, in the θ direction the temperature distribution and heat flux is $\pi/60$. If we focus on only one of these cycles, the following geometry will result:

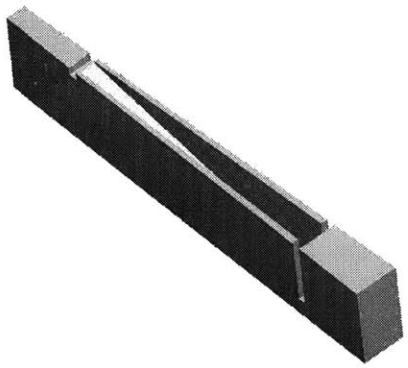

Figure 12: $\pi/60$ Slice of the bipolar plate

This depicts a groove with two halves of a wall, one on each side of the groove. Each wall is then .5 of a degree thick and the groove is 2 degrees wide. If we repeat this geometry 120

times and put them together side by side, the result is a full bipolar plate minus the gas-port holes.

Since the point of interest is really only the effect of the groove on temperature distribution, the gas ports will be neglected and the model that will be analyzed will be the following:

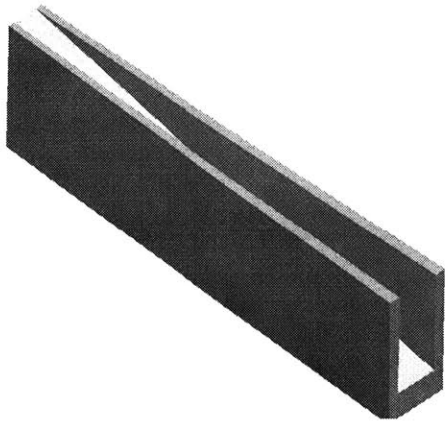

Figure 13: Simplified Slice

This simplifies the model greatly and allows a much faster analysis while that focuses on the important aspects of the model. This slice will be what is considered in the finite element analysis for this report.

This slice could be further divided into two parts. If one imagines a plane running vertically along the radius and in the middle of the groove, for any position inside this plane $dT/d\theta$ would be zero. On either side of this plane, for a given distance perpendicularly, there would be equal but opposite heat fluxes. For simplicity, this analysis will not further divide the slice. Instead, it will be left as is and the outcome will be analyzed in the results. See Plot 5.

5.3 Descretizing the slice into its elements

To analyze the slice, it must first be divided into elements. Each element will be analyzed for heat flux and temperature. This portion of the analysis was done on Proengineer Mechanica. The entire bipolar plate was made on Proengineer so it was relatively simple to create the slice model and export it to Mechanica. The software divides the slice into elements automatically as in figure14.

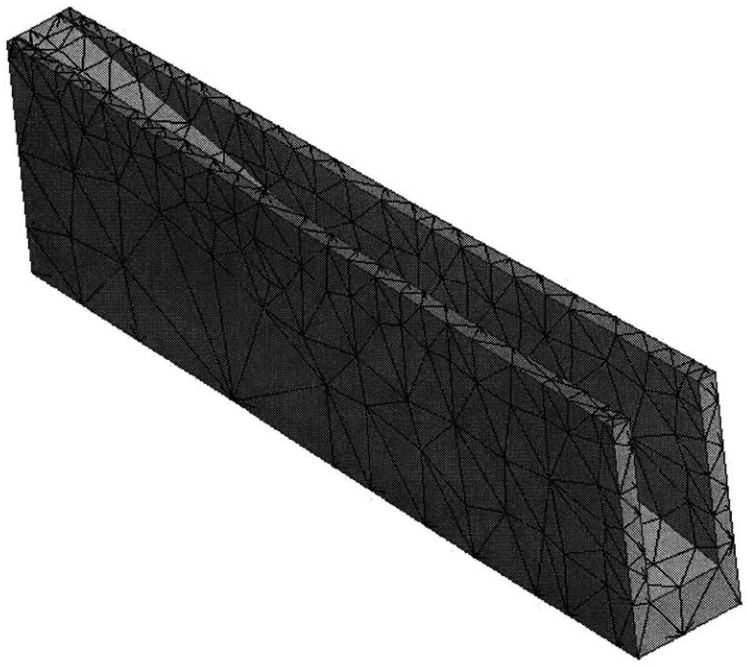

Figure 14: Descretized slice

It is very important to choose an aspect ratio for the elements so that every part in the interior of the model is accounted for. Choosing an aspect ratio that is too high, or too low may result in model errors as in figure 15.

If the aspect ratio is chosen to be at least 6, of the elements created with these settings, 3% of them are generated with misshapen geometry—that is to say, the ratio of their surface area

to their volume is unsatisfactory, and would therefore be discarded in the analysis by the software. This is undesirable because this would create areas of discontinuity inside the solid. The model in figure 14 uses an aspect ratio of at least 7 and does not show any errors.

5.4 Boundary Conditions

Boundary conditions must now be applied to the slice in order to perform any sort of analysis on it. But first, a nomenclature for each surface of the slice is necessary in order to more accurately explain the boundary conditions. The following figure depicts the important surfaces of the slice. An appropriate boundary condition will be associated to each of these surfaces. By symmetry, the conditions on one side of the slice will be the same on the congruent opposite side of the slice.

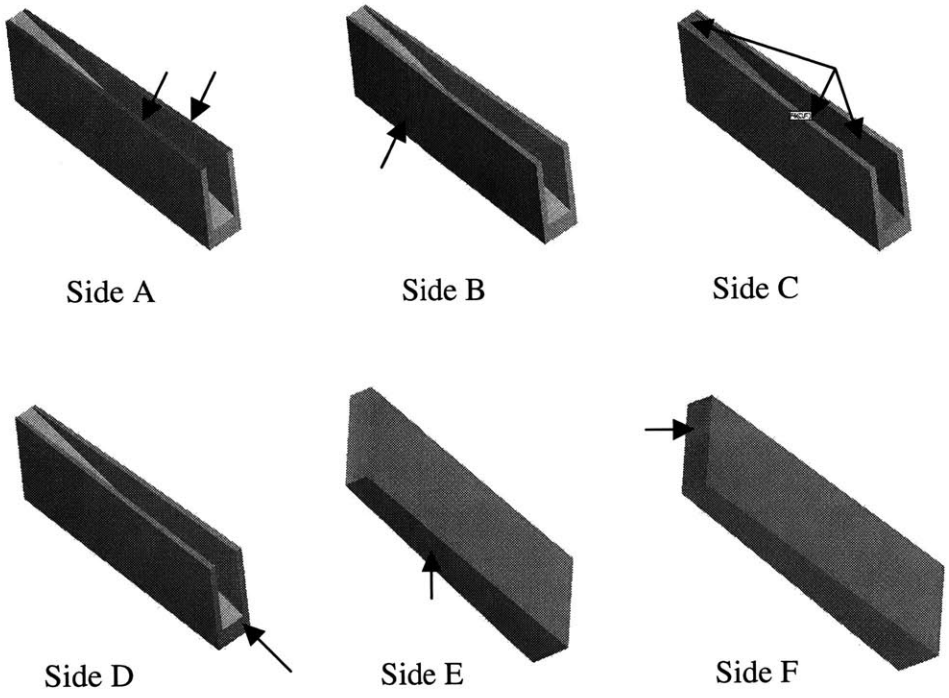

Figure 15: Nomenclature for the different sides of the slice

Note, Side A consists of the two upper surfaces of the slice; Side C consists of the 3 walls which constitute the inside of the groove; and the side opposite side B (Side B') is left out of the nomenclature because, from symmetry, it is equal and opposite to side B.

As for the actual boundary conditions, Sides A and E will be in direct contact with the electrodes. The reaction that takes place inside of these electrodes (by experimentation) outputs about 5 watts of heat. Therefore, on both these sides will be a constant heat flux of 5watts/(its corresponding surface area). These combine to a total of 10 watts for the whole body. Side A has a calculated surface area of about .11 in^3. Side E on the other hand, has a total surface area of about .33 in^3.

All of the surfaces of Side C, Side B, and Side B' will be considered adiabatic. For Side C, this is because the graphite (which is an excellent conductor) is not in direct contact with the electrodes. Instead the 5 watts is going into the steam produced. This, in turn, condenses and exits via the water removal ports. The heat of condensation is drained by the water removal ports to the water-reservoir. For this reason, in comparison to other heat fluxes, the heat flux into these surfaces will be considered negligible and the boundary condition for this surface is adiabatic.

As for Sides B and B', these will be considered adiabatic because they coincide with one another and if there was any heat flux between them, then the third assumption would be nullified: there would be heat transfer in the theta direction.

Finally, Sides D and F will have a constant steady state temperature of 300Kelvin, and 500Kelvin respectively. These temperatures were deemed acceptable environmental conditions for the produced fluid and the temperature of the outer wall of the casing which is being cooled by brine, mud, and sea water.

The slice, with all of its boundary conditions (as in figure 16) is now ready to be analyzed.

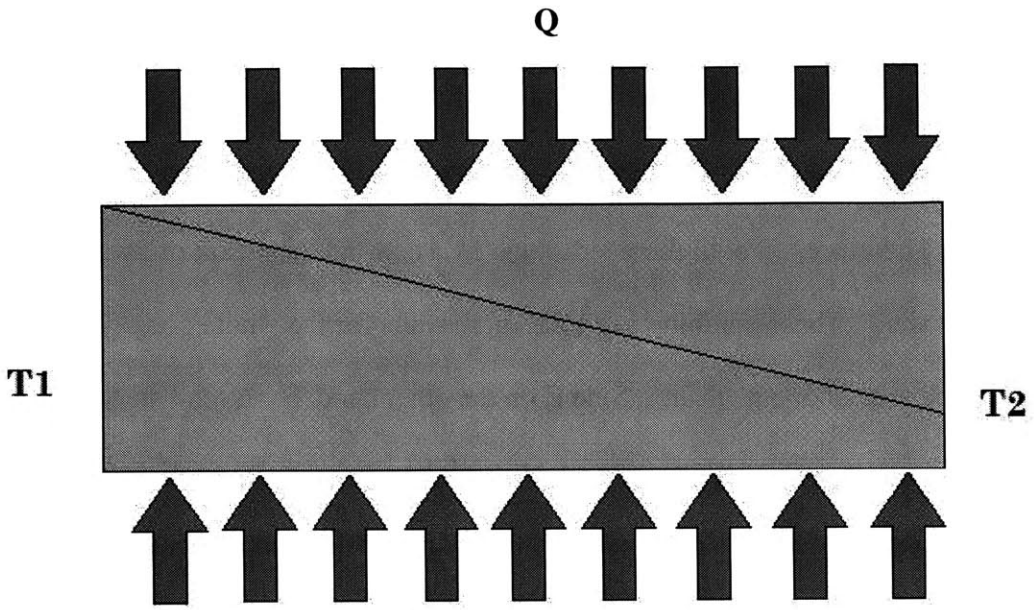

Figure 16: Slice with the corresponding boundary conditions

5.5 Results: Temperature distribution

The results of the finite element analysis are given in the next few pages as plots. There are several different types of plots using different techniques to display the results. One is the continuous tone fringe, which can be seen in the first temperature distribution plot. This consists of continuously changing colors signifying movement in the temperature. In this study, colors with lower wave-length (red) will signify something is hotter, while colors with lower wavelength (blue) will signify something cooler (less hot). The legend gives a good definition to temperature by associating it to a color.

Another technique is to use isoplanes. Isoplanes are denoted by contours of the same color and represent regions of continuously equal value (such as stress, strain, temperature, flux,

etc.). These are useful when demonstrating flow. In this case, Isoplanes will be used to demonstrate planes of constant temperature or heat flux.

The following plots are the results of the finite element analysis. The first plot is an illustration of the temperature distribution throughout the slice. The temperatures are depicted in the units of Kelvin.

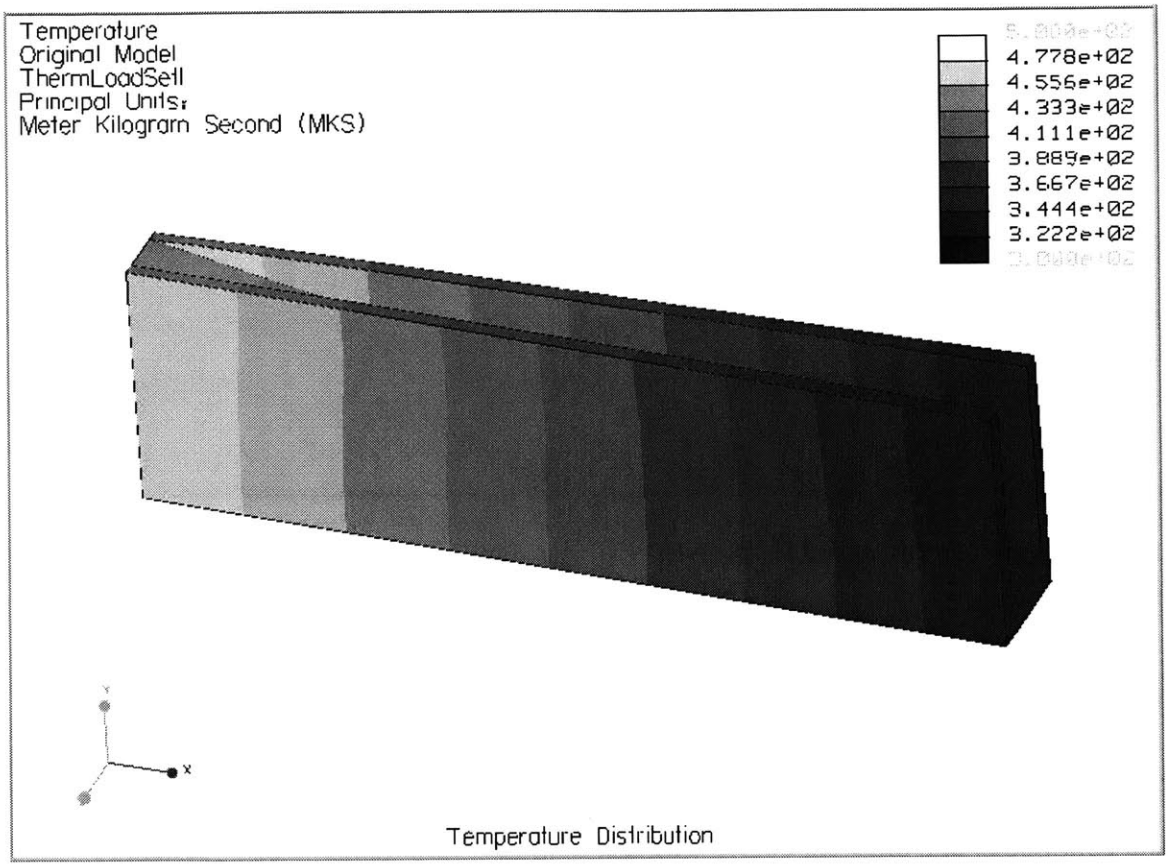

Figure 17: Temperature distribution (Kelvin)

As is clearly visible, the temperature changes steadily between the higher temperature 500 degrees Kelvin, to the lower temperature of 300 Kelvin. Figure 18 depicts this same temperature distribution using isoplanes.

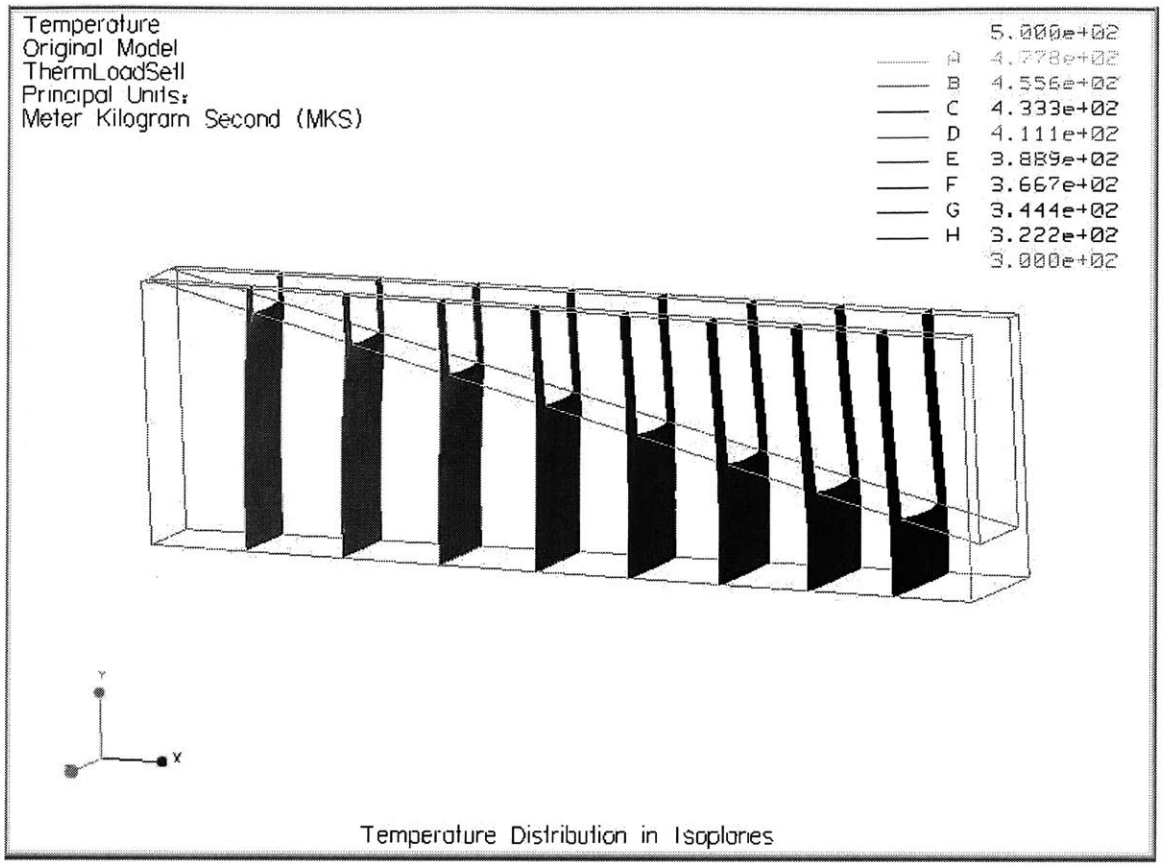

Figure 18: Temperature distribution (Kelvin)

Taking a closer look and using isoplanes, as in the second plot, one can see that the planes are not perfectly vertical. They bend slightly where the walls meet the bottom of the groove and continue in at a different angle. The fact that the isoplanes are nearly vertical (the bend in the planes is almost indistinguishable) means that difference in conduction is clearly negligible, however it does depict a very important factor: that the extremely high thermal conduction of the graphite carries the heat away easily with little regard to geometry. What this means is that, if necessary, a cheaper, more manageable material (such as stainless steel) with a lower thermal conductivity may be suitable. This will be discussed in further detail in the feasibility section of this report.

5.6 Results: Heat Flux

This section demonstrates the relevance of each component of the heat flux. This is important because it demonstrates the heat flux's dependence on direction for the given geometry. If it is found that the heat flux's component in the Z direction or Theta direction is small compared to the component in the R direction, then the assumptions made in the 1-D and 2-D models will hold up. The results of this analysis were obtained by plotting the heat flux with isoplanes (planes of constant heat flux) to get the general idea of how the heat flows in the geometry.

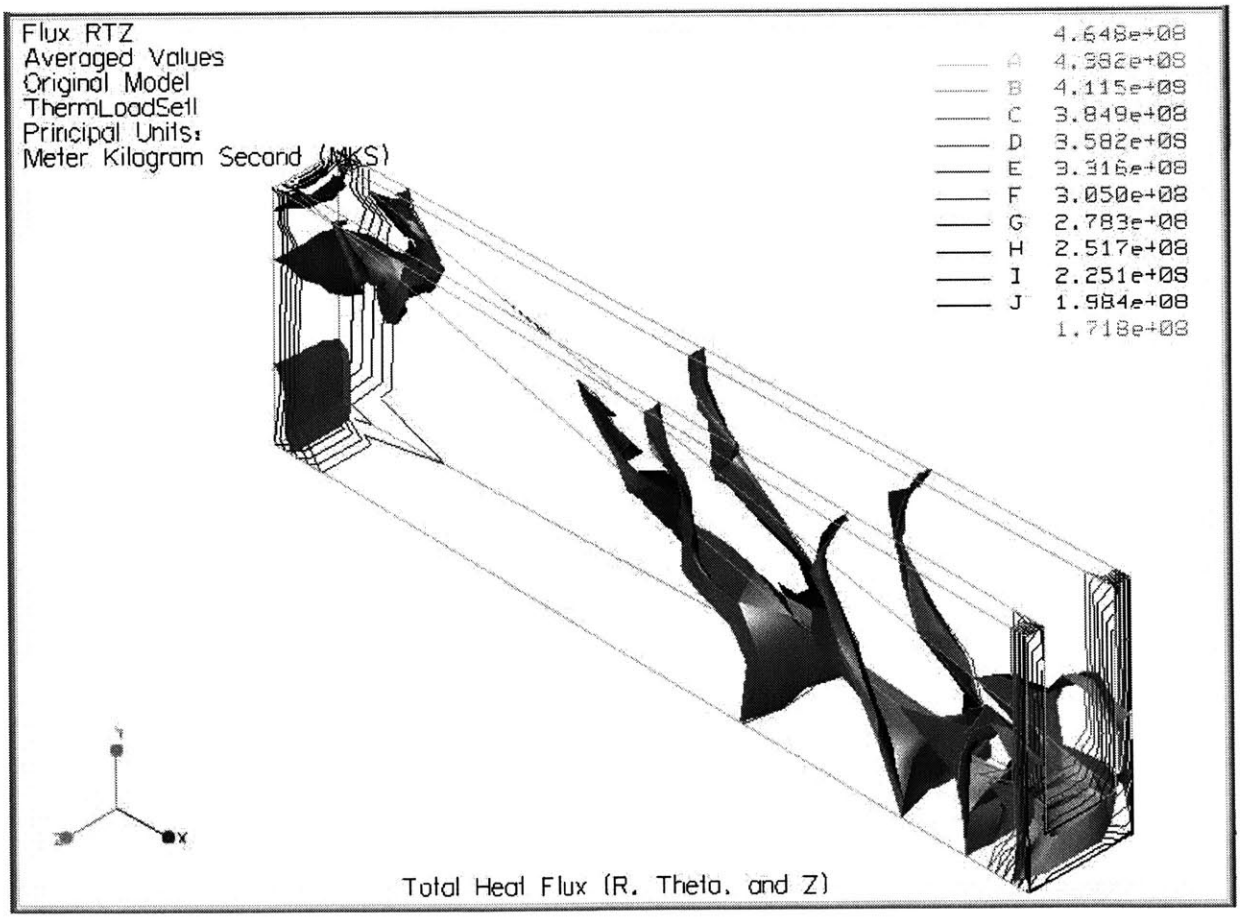

Figure 19: Total Heat flux (J/m^2)

The total heat flux is seen here as it varies through the geometry. The planes inside the solid represent planes of constant heat flux and their shape gives a sense of the general flow of heat. If this is compared with the heat flux component in the theta direction, there are several noticeable features that demonstrate that the component of heat flux in the theta direction plays a small role in the total heat flux:

1) The magnitude of the highest value of heat flux in the theta direction is about 10 times smaller than the magnitude of the lowest heat flux in the total heat flux.
2) The shape of the isoplanes in the Theta heat flux look nothing like the shape of the isoplanes of the total heat flux.

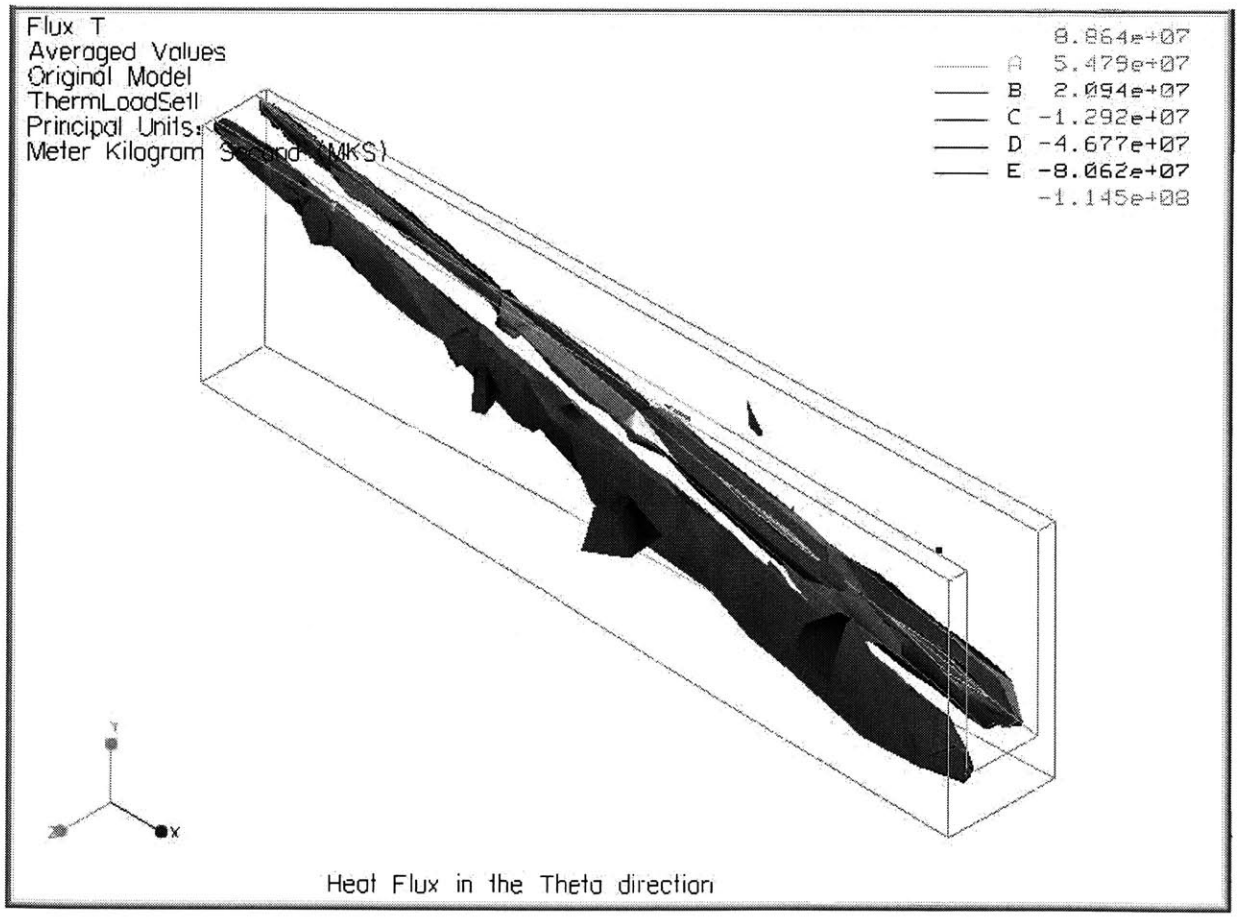

Figure 20: Heat Flux in Theta (J/m^2)

This same approach can be taken to compare the flux in the z-direction to the total heat flux. The result of this comparison is similar:

1) Note first the magnitude of the largest heat flux in this model. It is still an order of magnitude smaller than the total heat flux. This suggests that the total heat flux has little dependence on the z-direction for this geometry.
2) Also, the shapes of the isoplanes are still completely different from the total heat flux plot. This suggests that the effect of the z-component of flow is small.

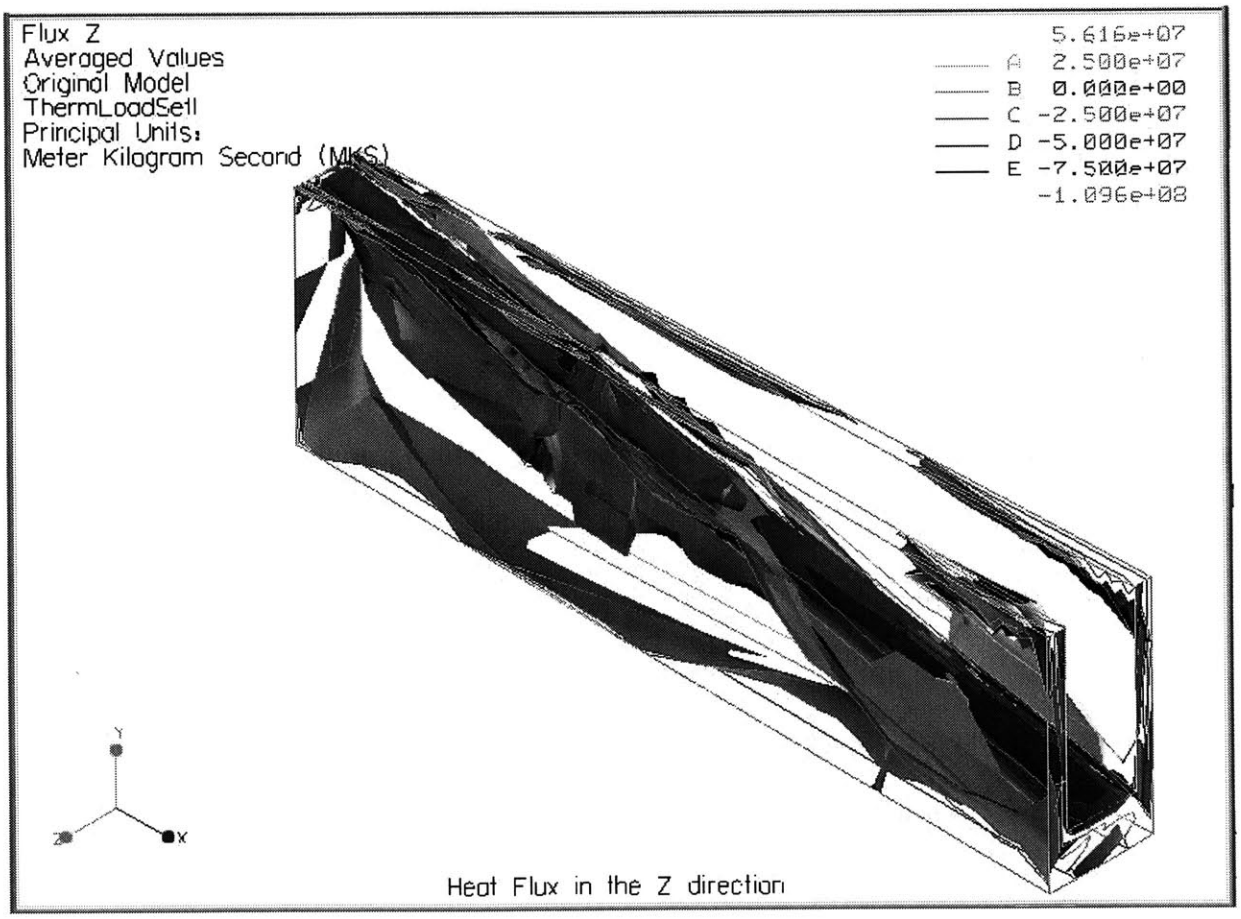

Figure 21: Heat flux in Z (J/m^2)

Figure 22 depicts a comparison between the radial component of heat flux (flux in R) and the Total Heat flux (flux in RTZ).

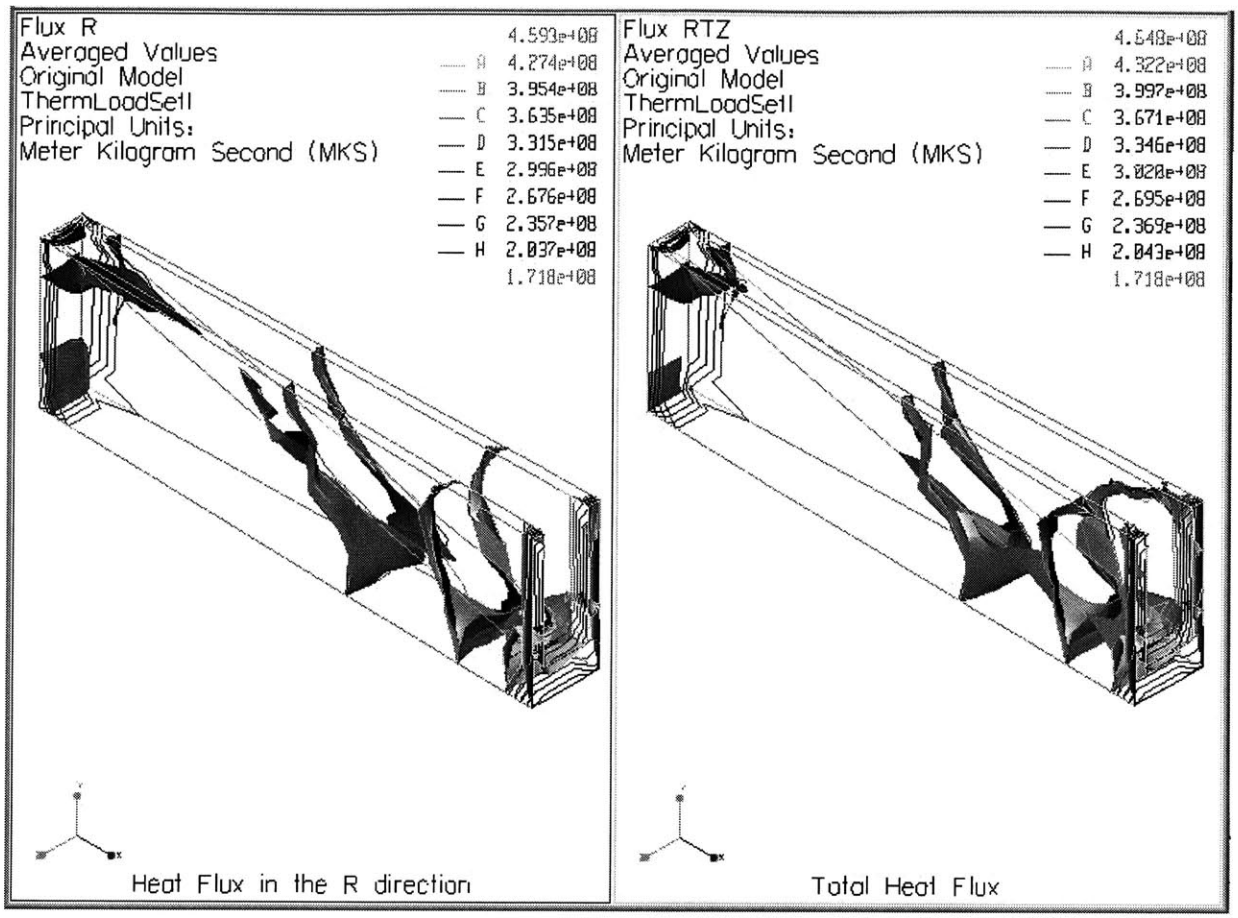

Figure 22: Comparison of Heat Flux in R and Total Heat Flux (J/m^2)

Some things to note:

1) Note first, the similarities between the two plots. They are almost identical.

2) Then, notice the similarity in the magnitude of the heat flux. The slightly lower magnitude in the plot for the R direction is due to the fact that we have neglected the smaller z and theta components. However, the magnitude is still within a reasonable range compared to the total heat flux.

These facts definitively validate the assumptions that the heat fluxes in the Theta and Z directions are small enough to neglect and therefore validate the 1-D and 2-D models.

6. Testing Phase

6.1 Introduction to the testing phase

As mentioned before, the thermal model above is based on a project that the Power Sources group at Schlumberger was working. The design of all of the components of the fuel cell had already taken place. The idea for this analysis was to create a thermal model of the system and then validate the model experimentally so that the group would have a basis for knowing the temperature inside the fuel cell.

Unfortunately, many complications arose in the experimental setup that slowed down the group's progress and prevented the experimental phase from taking place. In the following sections, these complications will be addressed. They are important factors that need to be considered in any fuel cell project but were neglected in this case.

Before trying anything with the large 18 inch diameter fuel cell, a small 2.5 inch diameter version was constructed. It consisted of up to 10 cells (less could be stacked if so desired) and did not have the annular hole running through the middle (see figures 23 and 24). This made handling much easier and if any problems were detected while running this scaled down version, the ramifications were greatly decreased.

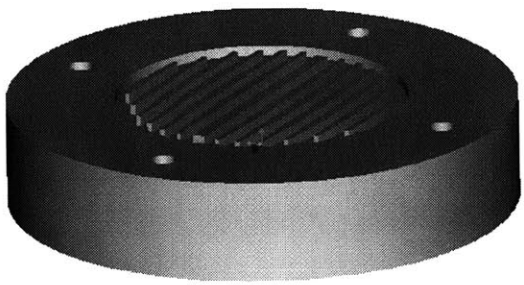

Figure 23: Bipolar plate for the 2.5" fuel cell

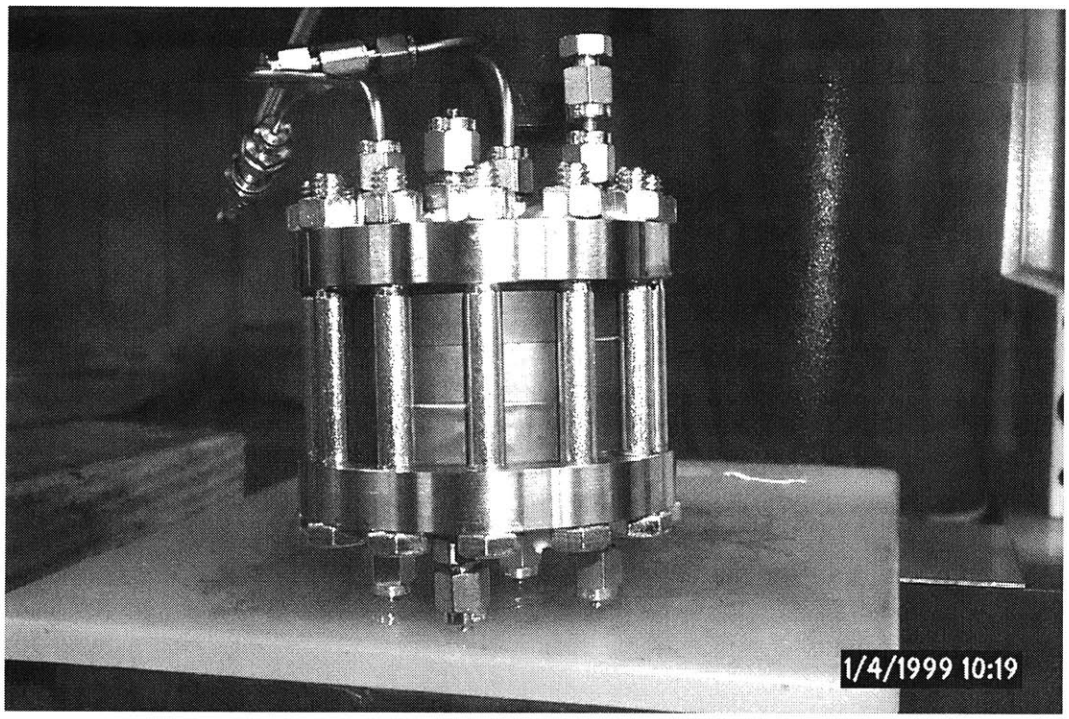

Figure 24: 2-cell stack with 2.5 inch plates

6.2 Sealing the cells

The issue of sealing the cells was by far the largest setback encountered during the period this project took place. Our system fed pressurized oxygen and hydrogen into the cells of the fuel cell via gas ports so it was necessary to have a seal between the both sides of the membrane and the bipolar plates (see figure 23).

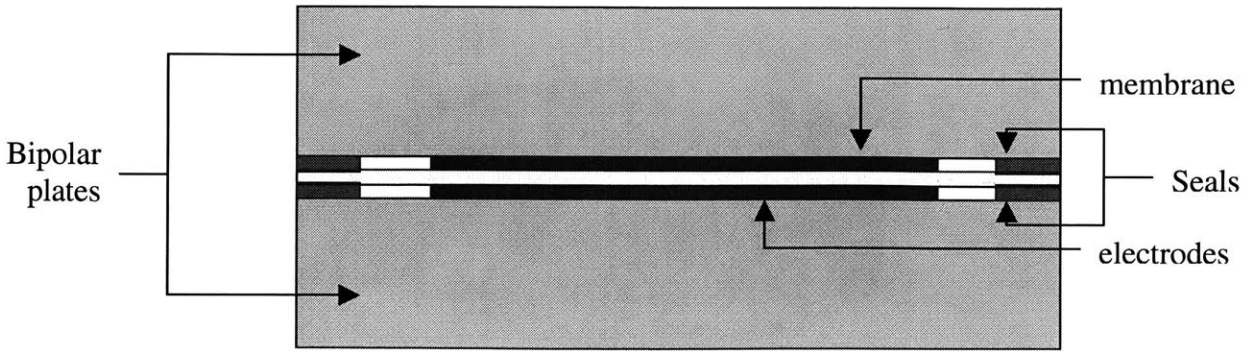

Figure 25: Cross-Section of one cell in the 2.5" fuel cell

Flat Gore-Tex gaskets were cut out with the dies pictured in figure 26.

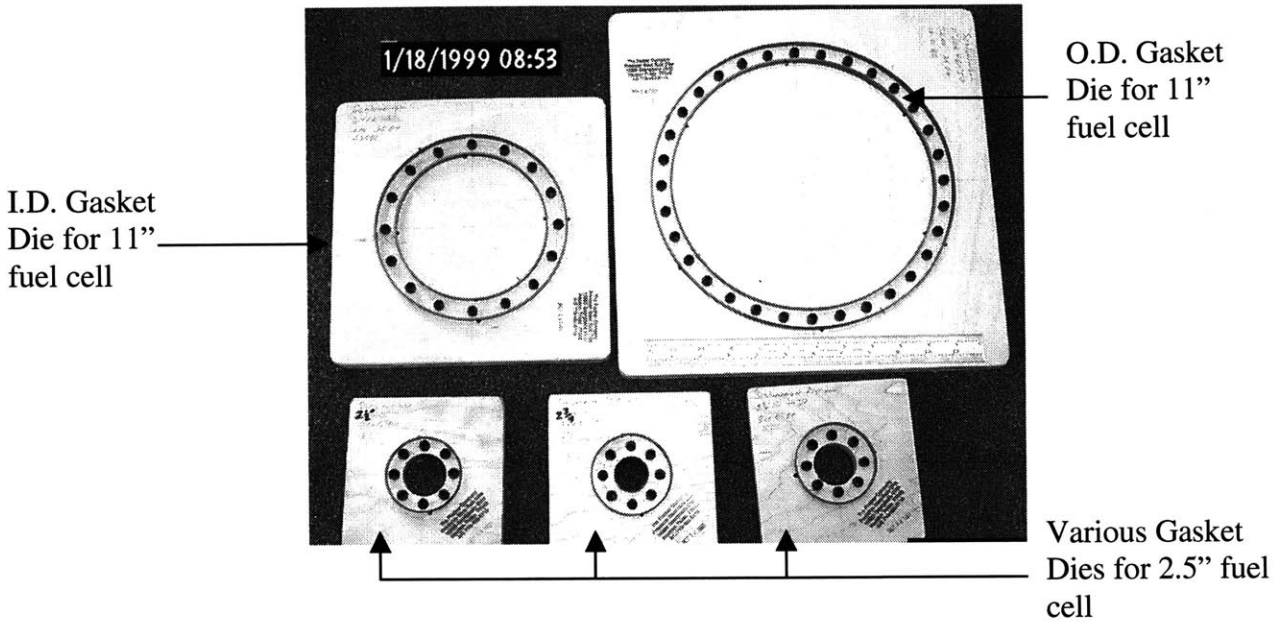

Figure 26: Gasket cutting dies

According to the engineers at goretex this material would create a bubble tight seal for hydrogen if it was compressed with a pressure of 2.4 KPSI. For the area of 3 in^2 for the gasket, an axial force of 7,300 lbs. was necessary from the bolts. The problem was that the engineers that designed the plates only made 4 quarter inch bolt holes. This meant that each bolt would carry 1,825 lbs. For such small bolts, this was impossible.

I designed the stainless steel end-plates depicted in Figure 27 sandwiching the entire stack. These endplates consisted of 12 holes through which insulated quarter inch bolts could fit to provide the load necessary to compress the gaskets. However, while that solved the problem of the axial load, it turned out that the system still leaked profusely. Figure 27 shows the leaking stack.

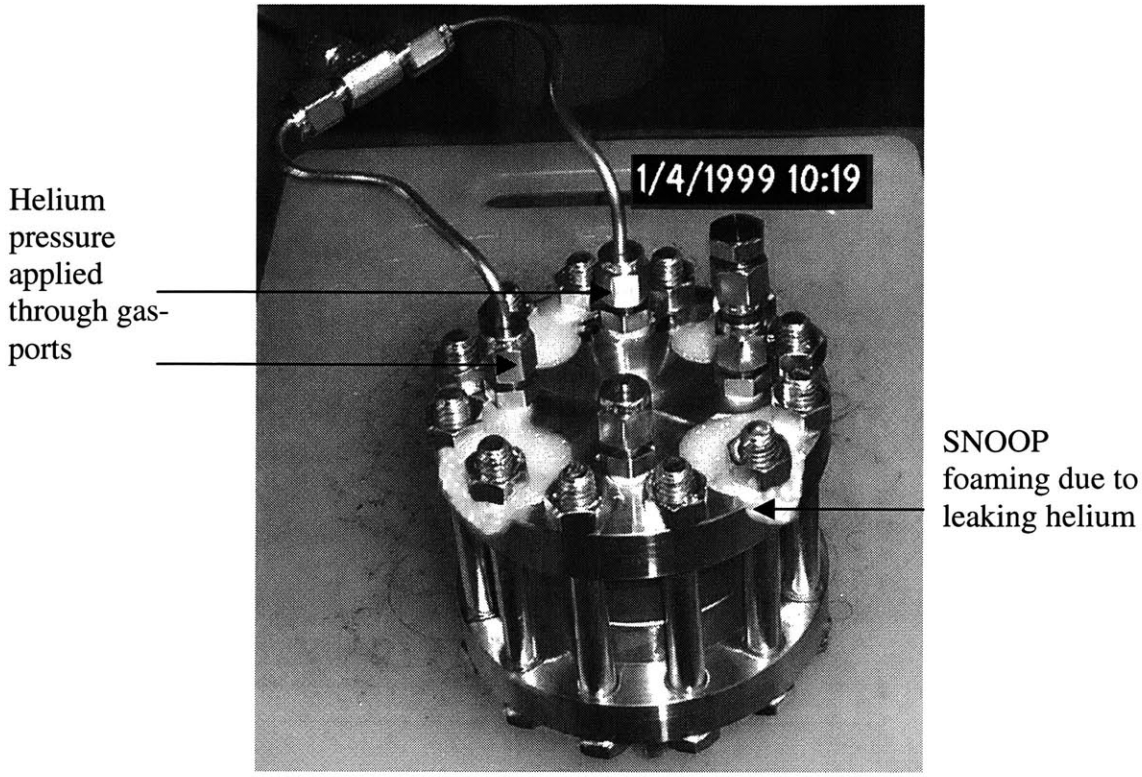

Figure 27: Foam exuding from the fuel cell due to a leak

The stacks were tested for leaks by using pressurized helium because it is inert (unlike the highly volatile hydrogen). A helium atom is slightly larger than a single hydrogen atom but smaller than hydrogen in its stable diatomic state. The stack was then sprayed with SNOOP ™ (which is the commercial name for a brand of soapy water used to detect leaks). SNOOP ™ creates many small bubbles when a leak travels through it creating highly visible foam. After about 5 seconds of being under only 10 PSI, the system would be covered in foam.

It turned out that the reason for this leaking was that the bipolar plates themselves were highly porous. Graphite has a molecular structure that, to a hydrogen atom, is extremely porous. The bonds between the carbon atoms are so long that they provide little barrier to pressurized hydrogen. To counter this effect each plate was sealed with a proprietary coating and baked as a part of its manufacturing process. Weather the porosity of the plates after being baked with the

coating was a mistake in manufacturing or a deficiency of the coating itself was never determined.

It was then decided to identify the bipolar plates that leaked the least and perform preliminary tests with as many cells as could be assembled with these plates. A stack of 2 cells was the end result. However, there was still foam exuding from the seal interface between the bipolar plates and the gortex seal. It was determined later, by the engineers at goretex that the bipolar plates had too high a surface finish to create a seal. The Gore-tex gaskets are composed of expanded PTFE (PolyTetraFlouroEthylene). This is basically PTFE with millions of microscopic bubbles throughout its interior creating a flexible foam. When pressure is applied locally, the area to which it is applied contracts and becomes hard. Since the compression is very local, the theory is that it fills any voids between in its interface and creates a moldable seal.

Graphite is very brittle. Therefore it must be machined slowly with very little surface force. When graphite is machined it creates a very fine dust that is used as a lubricant in many applications. This process creates an extremely high surface finish. When the Gore-Tex is compressed with this interface, the scale of the imperfections in the goretex is higher than the scale of the imperfections of the interface and larger than a single helium atom; thus creating a breach in the seal. Looking very closely at a compressed gortex gasket, one could identify the leak paths that the helium bubbles followed.

One solution to this problem which was not undertaken is to machine interference rings into the interface (see figure 28a and 28b).

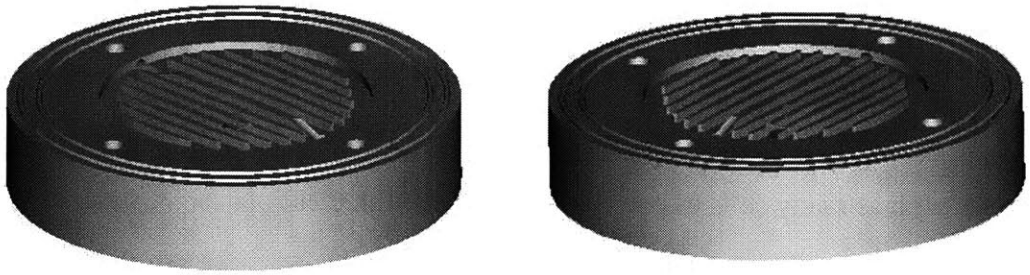

Figure 28 a) and b): Interference rings on bipolar plates

Figure 28a shows a bipolar plate with two bumps machined tangentially on the seal's interface. Figure 28b has the inverse of this pattern machined in the form of grooves. The bumps on 28a match with the grooves on 28b. This would create an area of very high stress concentration on the edges of the grooves which would create a more formidable barrier than in the previous case where the entire gasket was compressed uniformly. This possible solution and others are discussed in more detail in appendix A.

However with deadlines approaching, the group decided to look for a better sealing material with which to make gaskets. Using the same dies pictured in figure 26, new gaskets were cut out of over 12 different materials (see figure 29)

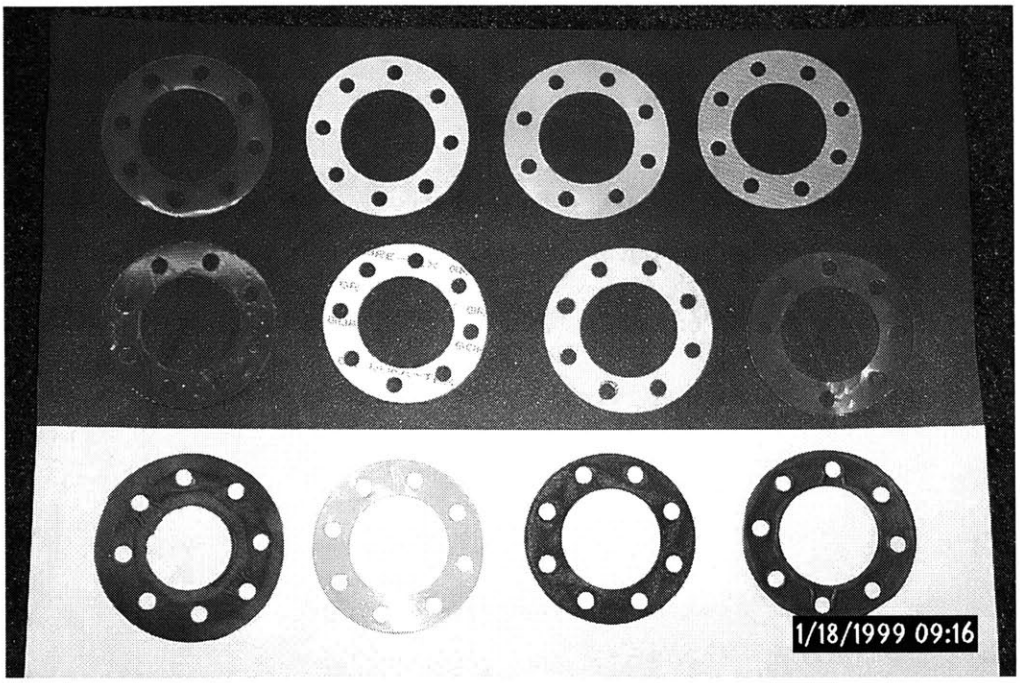

Figure 29: Gaskets cut from different materials

To name a few of these: Teflon, latex, PTFE, glass-fiber reinforced butyl, urethane, silicone, polyvinylchloride, PEEK (polyetheretherkeytone).

We found that the more malleable rubbers would extrude completely when too much stress was applied. Therefore, we tried glass fiber reinforced rubbers only to find that the helium would follow a strand of glass to the edge of the gasket and escape. When we tried harder polymers, we found that they did not deform sufficiently under the allowable stress (breaking point of the graphite plates) to stop the leaks.

The conclusion of this battery of experiments was that flat gaskets were the worst possible way to create a seal for such a small molecule. Out of all of the materials we tested, the goretex was the most suitable. Better methods for sealing this system are suggested in the Conclusions, however these were never tested.

The reason this leaking is not as big a problem in most PEM (Polymer Electrolyte Membrane) fuel cells in the world right now is because most of them do not run at pressure. The majority of fuel cells work at ambient pressure with hydrogen on one side of the membrane and ambient air at the other. For this reason, air-tight seals are not necessary. However this fuel cell is designed to work in much harsher and confined environments. It is necessary to have a supply of pure oxygen and hydrogen and it must be pressurized in order to meet the space constraints. Therefore seals are essential to the functioning of the system.

6.3 Oxygen/Hydrogen Safety

The entire group involved in the fuel cell testing was put through a week course on oxygen safety. As an oxidizer, oxygen dramatically decreases the auto-ignition temperature of many materials. This makes designing oxygen systems very important. Basically, an oxygen fire can result from one or more of the following:

1) Particle impact
2) Adiabatic compression
3) Frictional/Chemical heating
4) Mechanical impact
5) Electrical spark

Of these five, only 1), 2), 3) and 5) really apply to this system. Particle impact basically refers to a particle in a flow that impinges itself on a corner in the flow or a screen. This can cause a sudden release of energy that can ignite other components causing a disastrous chain

reaction. In this system it can occur on the startup when a regulator valve is opened and high flow rates occur over a short period of time. In the steady state, however, the system consumes hydrogen and oxygen at a relatively slow rate and it becomes a non-factor. To counter this all that would be necessary is to open valves slowly.

Adiabatic compression is just the opposite. This can occur when flow is suddenly stopped and pressure builds in the piping just before the valve momentarily. As pressure builds, temperature can rise and if the heat flow rate is relatively low, the heating could spark an ignition. Again, this is a non-factor at steady state, but when closing valves it is always a good idea to shut them slowly.

Chemical heating is probably the most dangerous for this system. When an exothermic reaction takes place (i.e. hydrogen and oxygen combine to create water) heat is released. This heat can cause problems for the system in three ways. First, heat reduces electrical conductivity thereby reducing the power output of the fuel cell. Second, heat can ignite a material in an oxygen rich environment. And lastly (and most dangerously) heat can rupture the membrane which separates the hydrogen and oxygen which can cause an explosion.

Finally, since this is an electrical system it is very important to keep sparks and charge carrying objects out of the exposure of oxygen. For this reason, all of the gas input lines and charge carrying surfaces are well insulated.

As a further precaution, all of the testing was to be done in explosion proof bays that were located about 100 yards from the office buildings. These bays were built with concrete cinder blocks and steel reinforcements. The oxygen and hydrogen tanks had to be separated by at least 25 feet outside of the bays and the gas was piped in using oxygen clean stainless steel piping.

6.4 Preliminary testing

Figure 30 is a picture of the setup which was to be tested.

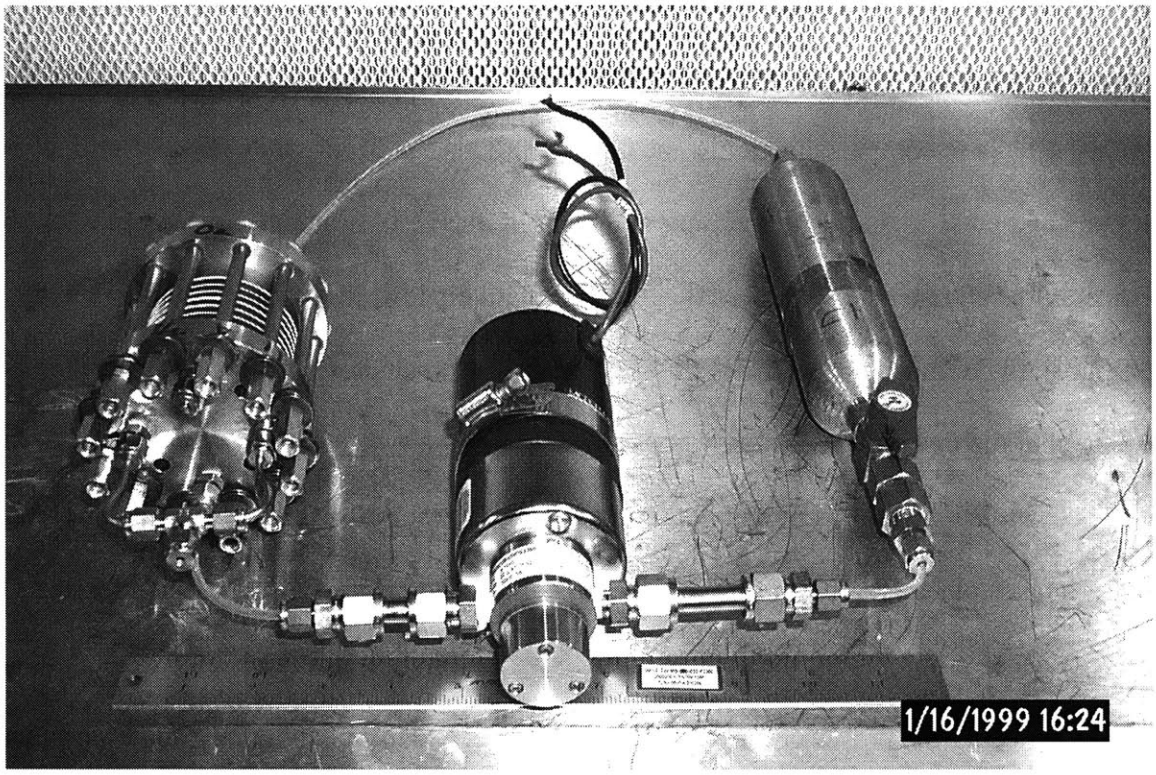

Figure 30: System to be placed in oven for testing

On the left, is the fuel cell stack; the cylinder in the middle is a gear pump; and the cylinder on the right is a water reservoir. The connectors (not pictured) run hydrogen and oxygen through the cells and create an electrical potential is created by the chemical reaction between the first and last bipolar plate. Each plate is insulated from the next by the seals and the membrane. The result of the reaction is voltage and water.

The water that is created in the cells is pulled to the bottom of each cell by gravity. The gear pump, which turns on periodically, pulls the water out and stores it in the reservoir. The whole system was to be placed in an oven inside one of the explosion-proof bays. The oven was

to maintain a constant temperature for three weeks. This preliminary testing was to provide a frame of reference for fuel cell performance. Fluctuating temperatures and pressures would then be added to simulate a down-hole environment. Finally, the analytical model presented in this report would be tested in a more complex setup involving the annular fuel cell.

Since this fuel cell dealt with pure pressurized oxygen and hydrogen, experimentation had to begin at a very basic level. As mentioned previously, most fuel cells function with hydrogen at atmospheric pressure on one side of the membrane; and air, blown in with a fan at the other side. This eliminates the need for pressure seals on either side of the membrane. Since the pressure differential across the membrane is minimal, the membrane sees no net force.

When running pressurized gasses, however, maintaining equal pressures on either side of the membrane is critical. Three different membrane thicknesses are manufactured: .004, .006, and .008 in. With electrical conductivity being inversely proportional to the thickness of the sheet (the thicker the sheet the longer it takes to transport an ion from one side to the other), the thinnest is preferable. However, the thinnest one can only withstand a 1 PSI pressure differential. The thickest can withstand a little more (about 3 PSI) however it is still very important to manage the pressure on either side accurately.

Figure 31 is a schematic of the control box that was designed by the technicians to control the pressures on either side of the membrane. Inside the box, the top regulator controlled the pressure of the hydrogen, the middle regulator controlled the flow of argon, and the bottom regulator controlled the flow of oxygen. Two very key aspects of these regulators caused the preliminary testing to fail:

1) The gauges on the hand-regulators chosen for the control box measured pressure in increments of 50 PSI. Based solely on the error intrinsic to the gauge, the membrane was destined to rupture.
2) All of these regulators are independent of one another. Therefore, even if the regulators were changed to measure to an accuracy of 1 PSI, it is nearly impossible to have the same pressure of oxygen as that of hydrogen at the same time.

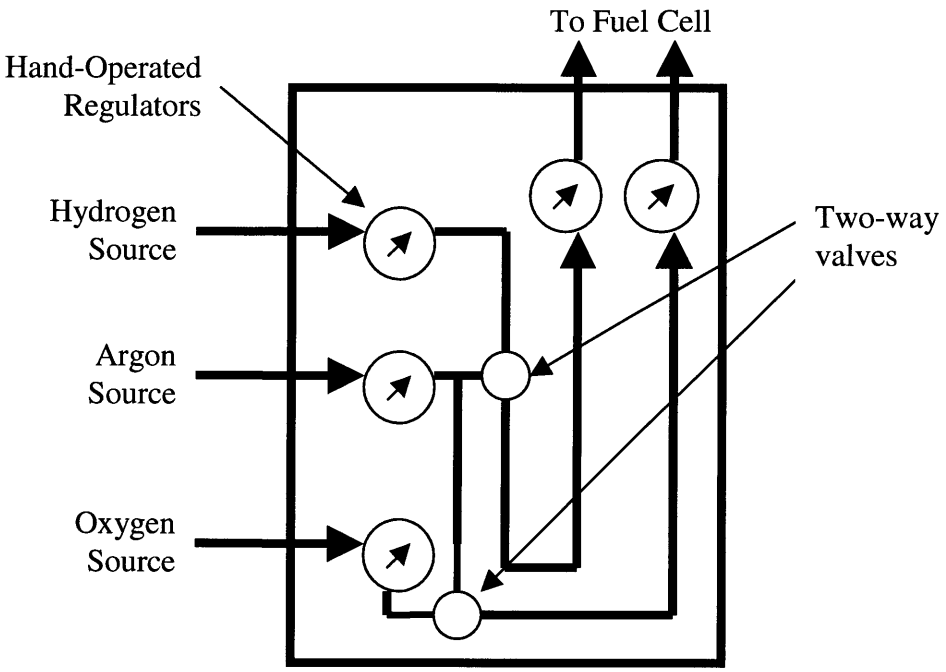

Figure 31: Gas-flow Control box

Because of the two points mentioned above, it is virtually impossible (because of human error) to maintain the kind of accuracy in differential pressure that the membranes demand for structural integrity. As a result, this opens the door for catastrophic failure: Oxidizer + Fuel = Possible explosion. As a result of these design errors the membranes did rupture causing high

localized heating. Nothing exploded, however the scare was enough to send the engineering team back to the drawing boards to design a better gas flow control box.

7. Conclusions

7.1 1-D model

The 1-D model was a success in that it demonstrated the effects of the annular bore inside the graphite plates. It served as a good foundation for the analytical portion of this report. However, had the thermal conductivity of graphite not been so high, the 1-D model would have been insufficient.

Indeed, one of the suggestions to be mentioned is to consider other materials to manufacture the bipolar plates. Suggestions to improve the design will be discussed in a moment.

7.2 2-D model

The 2-D model successfully proved the assumption of the 1-D model that the water-removal slope in the slots negligibly affected the flow of heat. In other words, heat flux in the z direction is negligible. As with the 1-D model, this is a good assumption because of the high thermal conductivity, however it is necessary to consider all geometries when dealing with materials that are more susceptible to heat accumulation.

7.3 3-D model

The 3-D model successfully proved the rest of the geometrical assumptions made in the 1-D model and the 2-D model. Specifically, heat fluxes in the theta and in the z directions are negligible.

However, this model does have its limitations. To actually employ this model, it is necessary to accurately predict the internal and external temperatures of the fuel cell. This model

is based on the boundary conditions on the inside and outside of each plate. In order for this model to work, it must be put in series with the convection conditions on the interior of the annular bore and on the exterior of the cylinder. However, since these conditions were still yet to be determined, they have been left out of this report.

7.4 Experimental Phase

This phase was unsuccessful in many ways for many reasons. However it managed to successfully orient the group towards what the main goals of this project are: to have a functioning fuel cell that can operate with the proposed geometrical constraints under the imposed environmental conditions.

In terms of the Chemical and Electrical engineering aspects, the project has met its demands. However, there is still much to be done in terms of mechanical engineering points, namely:

1) Design better bipolar plates: The current bipolar plates do not have large enough bolt holes to securely clamp the stack. Also, graphite is very brittle and a more suitable material is necessary in order to be able to withstand the abuse that will be dealt upon it in the field.
2) Sealing issues: Currently, the cells leak. The design must minimize the number and size of the sealing surfaces. Some possible solutions to this problem are listed in Appendix A
3) Packaging: The entire system must be designed to be manufactured and packaged in-lab and sent to the field ready to be connected. Some packaging suggestions are also featured in Appendix A

Appendix A: Suggestions for sealing cells

These solutions will assume that the porosity of the graphite plates will have been eliminated either by better manufacturing techniques or a change in material. These solutions have not been tested; however they are a possible solution in a pressurized fuel cell to eliminate leaking.

A.1: Interference rings

As previously stated in section 6.2, One solution to the sealing problem which was not undertaken is to machine interference rings into the interface (see figure 28a and 28b).

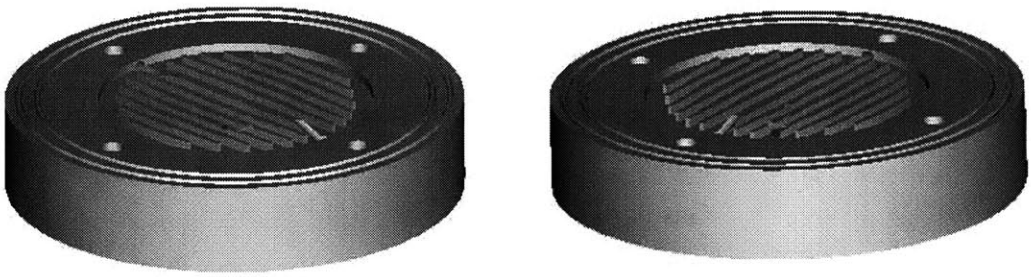

Figure 28 a) and b): Interference rings on bipolar plates

Figure 28a shows a bipolar plate with two bumps machined tangentially on the seal's interface. Figure 28b has the inverse of this pattern machined in the form of grooves. The bumps on 28a match with the grooves on 28b. This would create an area of very high stress concentration on the edges of the grooves which would create a more formidable barrier than in the previous case where the entire gasket was compressed uniformly.

Similar rings could be milled into the 11 inch bipolar plates to address leaking in the larger annular stack.

A.2: Molded Polymer Seals

This solution is similar to the one above in that it creates a more localized sealing surface. However in this case, slots are milled around the edges of the active area and around the gas ports. The slots around the active area are filled with a polymer (yet to be determined) that bonds directly with the graphite plates. This procedure will effectively remove 2 out of the 4 sealing surfaces in a cell. If successful, it completely eliminates leak paths between the bipolar plate and the seal; leaving only the surface between the membrane and the seal for gas to escape.

Figure 32 illustrates the slots to be milled for this strategy in the 2.5 inch fuel cell.

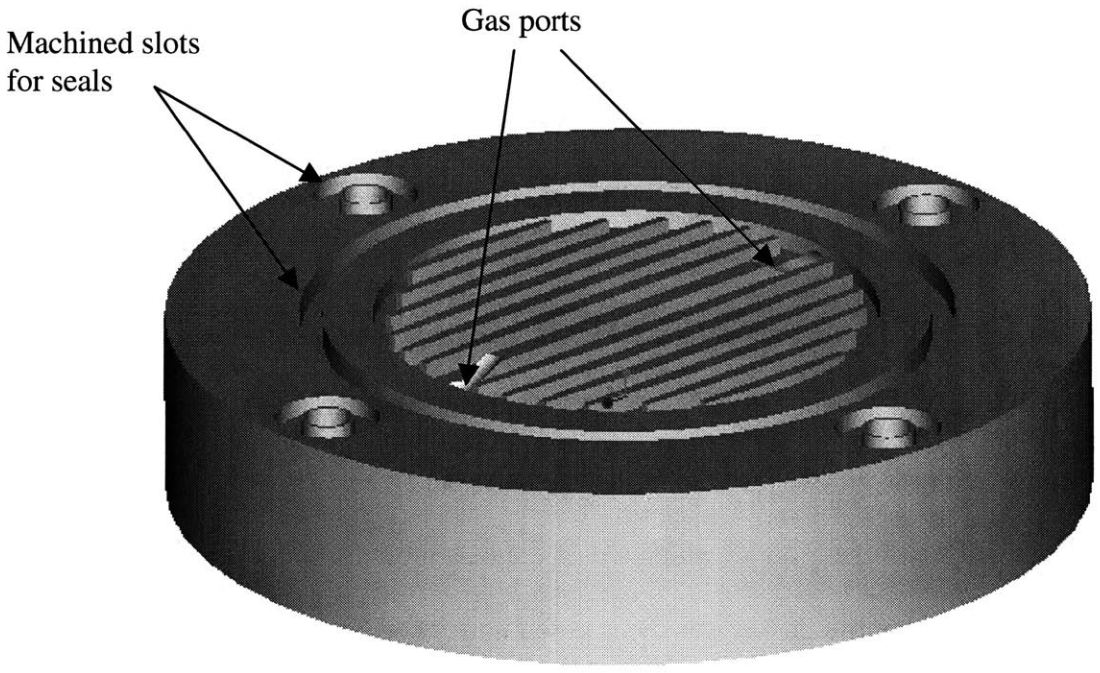

Figure 32: Machining to be done on 2.5 inch bipolar plate

Figure 33 depicts the polymer seal bonded in the machined groove. The gas-ports would be sealed by O-rings.

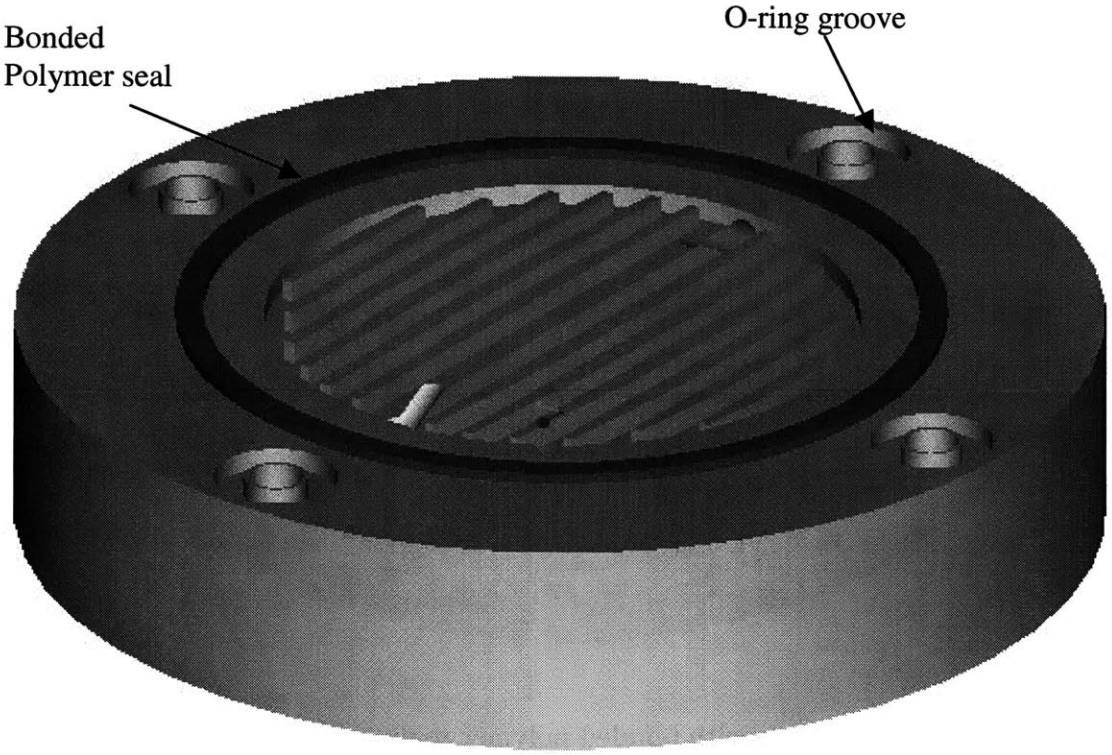

Figure 33: Molded polymer bonded to the slots

The gas ports are then sealed either with the same type of material, or with a single o-ring. The gasses are piped into the active area through a small hole that taps into the gas manifolds leading to the active area.

This idea can also be incorporated into the larger 11 inch fuel cell. Figure 34 illustrates.

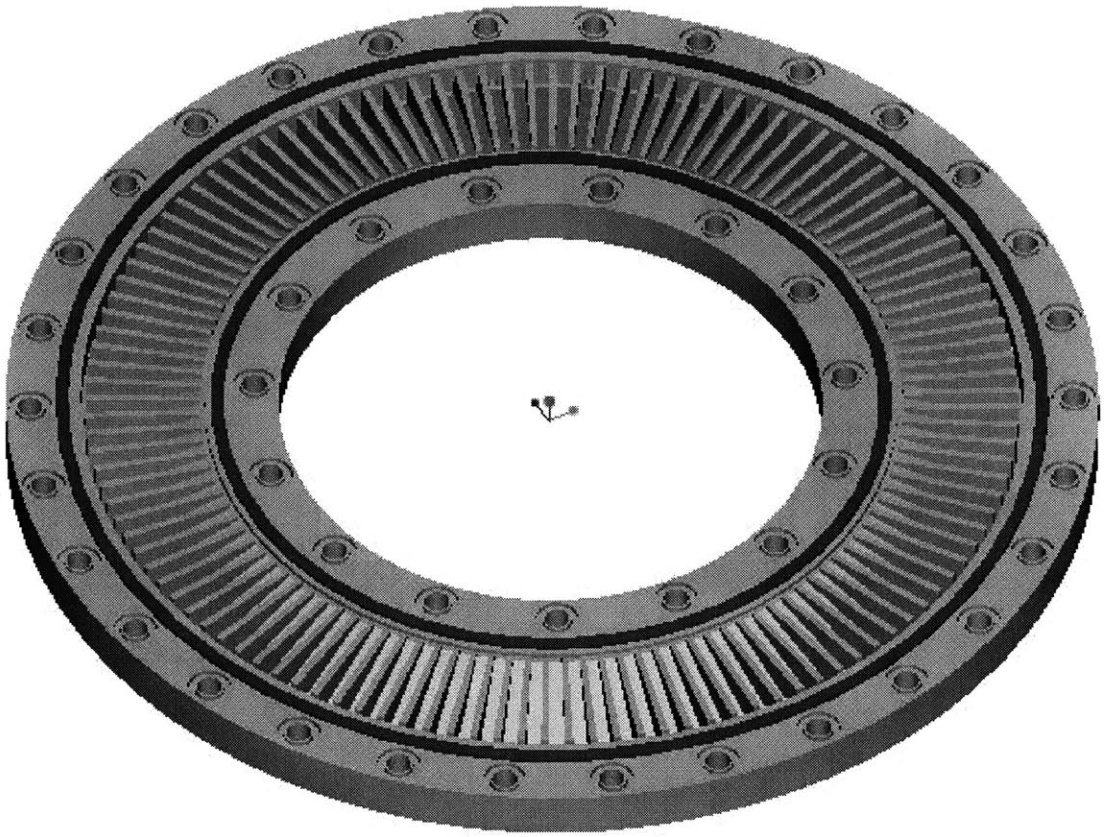

Figure 34: 11 inch bipolar plate with bonded polymer seals

A.3: Packaging

As mentioned in section 7.4, the entire system must be designed to be manufactured and packaged in-lab and sent to the field ready to be connected. This will prevent premature corrosion and ensure a longer life. The operations required to assemble and package a fuel cell are time consuming, delicate, and tedious. These procedures would be best followed in a controlled environment by very careful hands. The MEA's (membrane electrolyte assemblies) are very delicate and prone to tearing.

For these reasons, a robust package must be designed to facilitate deployment in the field. A suggestion for this packaging is illustrated in figure 35.

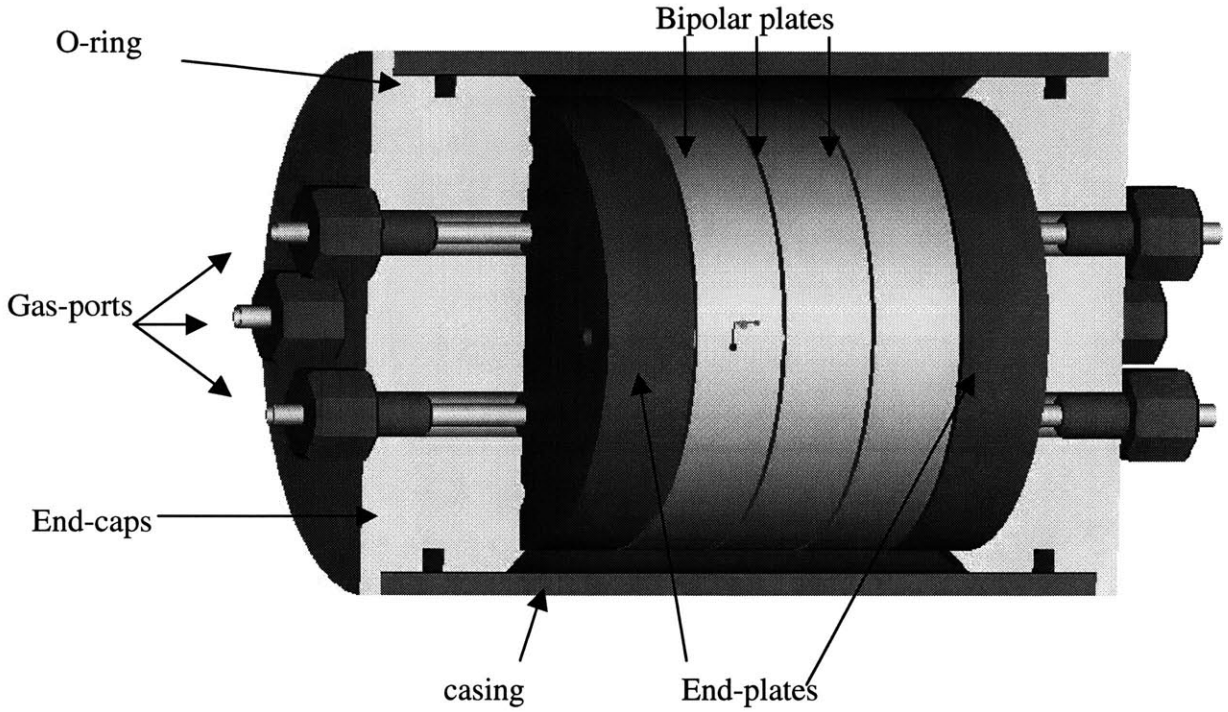

Figure 35: Leak-retardant packaging for fuel cell

This type of packaging can also prevent leaking in the cells. If a leak were to occur at some point in time in any of the cells, it would be adequately contained by the end-cap seals. The leak would eventually cause equalization of pressure between the outer casing and the cell thereby eliminating the pressure potential and thus eliminating the leak.

This is a simple idea manifested in a crude figure that would need much more engineering. However, the basic idea is robust and has much potential regardless of the type of sealing one chooses between the bipolar plates. This idea can also be incorporated into the 11 inch annular fuel cell. However, it is highly recommended that testing be carried out on the 2.5 inch fuel cell first.

Appendix B: Technical Information about Nafion ® membranes

The following pages were obtained from the Dupont Technical Department. For more information on the functionality and specifications of the Nafion® membrane, see the final page of this appendix.

Nafion®

perfluorinated polymer products

Equivalent Weight and Acid Capacity Measurements

A base titration procedure measures the equivalents of sulfonic acid in the polymer, which in turn determines the acid capacity or equivalent weight (EW) of Nafion® membranes and resins.

The procedure's calculation uses the weight of the "dried polymer" in the sodium salt form, since the alkali metal salts of Nafion® retain less water than the acid form' and provide values that are more reliable for the titration method.

Materials and Reagents

Titration grade potassium hydrogen phthalate (KHP, MW = 204.23)
1 liter 0.25 N or 0.50 N sodium hydroxide (NaOH)
Nafion® membrane, 3 samples, 0.25 g each or Nafion® pellets, 3 samples, 0.50 g each
Phenolphthalein (0.5 wt % in 1:1 2-propanol/water)

18 *MD,* deionized (DI) water
2 liters 2M hydrochloric acid (HC1)
2 liters 2M sodium chloride (NaCI)
125 mL Erienmeyer flasks
100 mL porcelain (Coors) funnel and vacuum flask
25 mL burette or auto-titrator
Mortar and pestle

Teflon® coated tweezers

' **A. Eisenberg and H.L. Yeager, *Perfluorinated lonomer Membranes.***

Base Standardization Procedure

1. Grind up 1 g of KHP to a fine powder using a dry mortar and pestle. Dry the KHP (in a weighing jar) in a vacuum oven at 40-70°C for 1 hour. Transfer to a dessicator to cool and for long term storage.
2. Weigh out, analytically (to the nearest 0.0001 g), 0.10 g or 0.20 g of KHP into three clean and dry Erienmeyer flasks. Add 50 mL of DI water to each flask and titrate the NaOH (0.25N or 0.50N NaOH, respectively) to the phenolphthalein (2 drops, persistent light pink color) endpoint.

Calculate the base normality ([NaOH]), using the following formula, and as an average **of** three replicates:

$$[NaOH] = \frac{m_{KHP}}{MW_{KHP} \times V_{NaOH}}$$

where m_{KHP}, MW_{KHP}, and V_{NaOH} are the mass (grams) and molecular weight of KHP and the volume (liters) of NaOH required to titrate the KHP, respectively.

Equivalent Weight and Acid Capacity Measurements

1. Acid exchange each of three Nafion® membrane or pellet samples in 125 mL Erienmeyer flasks with approximately 50 mL of2M HC1 for at least 1 hour. Decant the supernatant and repeat the acid exchange procedure. Use a porcelain funnel to catch any pellets that may decant. Add them back to the flask.
2. Rinse the samples in the flasks with DI water and soak them in approximately 50 mL ofDI water for at least 15-30 minutes. Decant the water and repeat rinse/soak two more times to remove excess HC1.

3. Add approximately 50 mL of 2M NaCI to each sample and let stand for at least 15-30 minutes. For pellet samples, also add 10 mL ofethanol. With gentle swirling, titrate the solutions with NaOH (0.25 N for 0.25 g membrane samples or 0.50 N for 0.50 g pellet samples) to the phenolphthalein endpoint. Estimate both start and end volumes to ±0.02 mL. A blank consisting of 50 mL of2M Nad (and 10 mL ofethanol for pellet samples) *may* also be titrated and the volume of base subtracted from the volume required to titrate the sample.
4. Rinse/wash the samples in the flasks with DI water and let stand in approximately 50 mL of DI water for at least 15-30 minutes. Decant the supernatant and repeat this step two more times to remove excess NaCI. Use a porcelain funnel to catch stray pellets. For membrane water uptake measurements (optional), proceed to step 5, otherwise go to step 6.

5. To determine the wet membrane weights (Na+ form), dry each membrane by gently wiping the surfaces with lint-free tissue and then weigh the membrane (analytically on a watch glass). Repeat this step two more times while allowing the membranes to equilibrate in DI

water for at least 5 minutes between drying/weighing. Calculate the average of three wet weight measurements for each membrane.

5. Decant the excess water from the membranes in the Erienmeyer flasks. Dry in vacuum oven (liquid N2 trap, $P < 1$ mm Hg) at 70°C for at least 2.5 hours or overnight using "house" vacuum (> 20 inches of Hg, gentle N2 purge). Quickly, transfer the flasks to a dessicator to cool before weighing.
With clean gloves or lint free tissue, quickly remove the flasks (one at a time) from the dessicator and weigh, using the analytical balance. Remove the membrane from the flask, with tweezers, and re-weigh the flask. Record the membrane "dry weight" as the difference between the two flask weights.

7. Calculate the EW (Na+ form) using the following formula and as an average of three replicates noting the standard deviation:

$$EW(gmol^{-1}) = \frac{Dry\ weight(g)}{V_{NaOH}(L)X[NaOH](M)}$$

8. Calculate[2] the EW (H_3O+ form) by subtracting 4 g/mol from the EW (Na+ form):

$$EW(H_3O+, g/mol) = EW(Na^+, g/mol) - 4\ g/mol$$

9. The Acid Capacity is calculated[3] using the following formula:

$$Acid\ Capacity\ (meq/g) = \frac{1000}{EW(H_3O+\ form)}$$

10. Calculate the weight percent water, as an average of three replicates, using the following formula:

$$\text{Weight Percent Water} = \left(\frac{Wet\_weight}{Dry\_weight} - 1\right) \times 100\%$$

[2] The Equivalent Weight (EW) value for Nafion® membranes and resins are reported in the "H_3O+ acid form", unless otherwise stated.

The Acid Capacity value for Nafion® membranes and resins are reported in the "H_3O+ acid form", unless otherwise stated.

Nafion®

perfluorinated polymer products

Conductivity Measurements of Nafion® Membrane

The conductivity of Nafion® perfluorinated polymer membrane is very important to its performance as a separator in electrochemical cells. Many factors in the manufacture and use of the membranes can affect the conductivity, so it is valuable to measure this property for quality control and technical service purposes. A brief description of the conductivity test method is given below.

The method utilizes impedance spectroscopy to measure the ohmic (real) and capacitive (imaginary) components of the membrane impedance. The membrane is boiled in D.I. water for one hour before testing. The cell is submersed in water at 25 ± 1 °C during the experiment. The plot of imaginary vs. real impedance (impedance plot or Nyquist plot) is shown below. The linear portion of the plot is extrapolated to zero capacitance, where the ohmic resistance is measured. From this value of resistance, along with the cell constant and the membrane thickness (measured wet), the conductivity in S/cm can be obtained.

Membrane Impedance

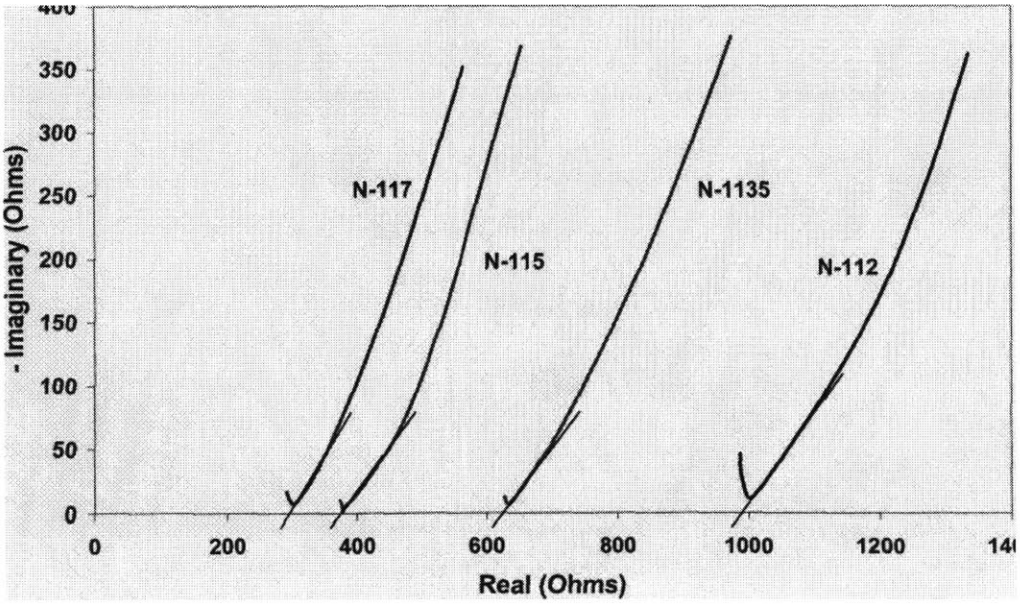

Measurement parameters: frequency range, 10^5 Hz to 1 Hz; 0 VDC, 10 mV (rms) AC.

Nafion®

perfluorinated polymer products

Nafion® Membranes NE-112, NE-1135, N-115, N-117

Description

Nation® membranes are non-reinforced films based on Nafion® resin, a perfluorosulfonic acid/PTFE copolymer in the acid ($H^{[1]}$) form. Nafion® is widely used for Proton Exchange Membrane (PEM) fuel cells and water electrolyzers. The membrane performs as a separator and solid electrolyte in a variety of electrochemical cells which require the membrane to selectively transport cations across the cell junction. The polymer is chemically resistant and durable.

Order and Packaging Information

Membrane dimensions are based on dry product conditioned at 23 °C and 50% Relative Humidity before cutting. The membrane's water content will affect its dimensions, and the change may not be symmetrical in the length, width, and thickness directions. In addition, certain conditioning steps performed by the customer also may affect the dimensions. Customers may wish to review their membrane treatment steps and dimensional requirements with a Nation® Technical Representative before establishing membrane shipping dimensions.

- Standard dry product dimensions for individual pieces include:
  - Width: 0.30m(min.) to 1.22m (max.)
  - **Length:** 0.30m(min.) to 1.22m (max.)

The membrane delivery package for cut pieces will depend on the size and quantity of the membrane order. Smaller-sized membranes are shipped flat, while longer lengths of individual pieces are shipped on a roll. The membranes are protected with a polyethylene wrap and inner packaging, then placed in shipping containers.

Standard dry product dimensions for roll goods include:

- **Width:** 0.30 m and 0.60 m standard roll widths, with 0.19 m (min.) to 1.22 m (max.) on special order
- Length: 50 m standard roll length

There is a 100 m^2 minimum order requirement for non-standard roll widths and lengths.

Membrane pieces or rolls can be cut to custom sizes, and special packaging provided at additional cost and/or delivery time. Please contact Nation® Customer Service for details.

Properties of Nafion® Perfluorinated Membrane

C. Hydrolytic Properties

Property	Typical Value	Test Method
Hydrolytic Properties		
Water content, % water[7]	5	ASTMD 570
Water uptake, % water[8]	38	ASTMD 570
Thickness change, % increase		
from 50% RH, 23 °C to water soaked, 23 °C	10	ASTMD 756
from 50% RH, 23 °C to water soaked, 100°C	14	ASTMD 756
Linear expansion, % increase[9]		
from 50% RH, 23 °C to water soaked, 23 °C	10	ASTMD 756
from 50% RH, 23 °C to water soaked, 100°C	15	ASTMD 756

[7] Water content of membrane conditioned to 23 °C, 50% relative humidity (RH), compared to dry weight basis.
[8] Water uptake from dry membrane to water soaked at 100 °C for 1 hour (dry weight basis).
'Average of MD and TD. MD expansion is slightly less than TD.

For more information about Nafion® contact:

DuPont Fluoroproducts
Nafion® Global Customer Service
22828 NC Highway 87 W
Fayetteville, NC 28306, U.S.A.

Telephone: (910)678-1380
Domestic U.S.A. only: (800) **436-1336**
Overseas: (910)678-1337
Fax: (910)678-1342

Nafion®

Only by DuPont

Bibliography

[1] Frank P. Incropera, and David P. DeWitt, Fundamentals of Heat and Mass Transfer, 4th edition, John Willey & Sons Inc. 1996.

[2] H.S. Carslaw and J.C Jaeger, Conduction of Heat in Solids, 2nd edition, Oxford Science Publications, 2000

[3] C.H Edwards Jr., and David E. Penny, Elementary Differential Equations, 3rd edition, Prentice Hall 1985

[4] Kenneth Wark, Thermodynamics, 3rd edition McGraw Hill, 1977